RSC Advances

From macro to micro: structural biomimetic materials by electrospinning

Journal:	*RSC Advances*
Manuscript ID:	RA-REV-05-2014-005098.R1
Article Type:	Review Article
Date Submitted by the Author:	25-Jul-2014
Complete List of Authors:	Ke, Peng; Tianjin Polytechnic University, Jiao, Xiao-Ning; Tianjin Polytechnic University, ; Key Laboratory of Advanced Textile Composites, Ge, Xiao-Hui; Qingdao University, ; Key Laboratory of Photonics Materials and Technology in Universities of Shandong, Xiao, Wei-Min; Donghua University, Yu, Bin; Tianjin Polytechnic University,

From macro to micro: structural biomimetic materials by electrospinning

Peng Ke[1] Xiao-Ning Jiao[1, 2*] Xiao-Hui Ge[3, 4] Wei-Min Xiao[5] Bin Yu[1]

1. School of Textiles, Tianjin Polytechnic University, Tianjin 300387, China
2. Key Laboratory of Advanced Textile Composites, Ministry of Education, Tianjin 300387, China
3. College of Physics, Qingdao University, Qingdao 266071, China
4. Key Laboratory of Photonics Materials and Technology in Universities of Shandong, Qingdao 266071, China
5. College of Textiles, Donghua University, Shanghai 201620, China

* Corresponding author. Tel.: +86 22 8395 5353; Fax: +86 22 8395 8287; E-mail address: xiaoningj@tjpu.edu.cn.

Abstract: Bionics provides a model for preparation of structural materials. Recently, the preparation of biomimetic materials has become an increasingly hot research topic. As an increasingly popular method for the fabricating micro/nano materials, electrospinning has been providing various products with controllable compositions and structures, therefore offering excellent prospects for construction of biomimetic structures. This review briefly described some artificial biomimetic structures which mimic living organisms with multilevel hierarchical structures from macro to micro, including plant-based soft tissue bio-materials, animal-based soft tissue bio-materials and animal-based hard tissue bio-materials, such as lotus leaf, moth eye, bone, etc, and related special functional properties, especially those fabricated via electrospinning. Moreover, the challenges in this field in the future, such as accurately analyzing about the structures of biomimetic materials, and designing composite functional or function-integrated materials have also been proposed.

Keywords bionics; biomimetic; hierarchical structure; electrospinning; property

1. Introduction

Over millions of years of evolution and selection, a large number of organisms, including plants, animals and biominerals in nature have possessed fascinating structures, almost perfect properties and functions, such as superhydrophobicity and self-cleaning of lotus leaves, anisotropic de-wetting behavior of rice leaves, attachment mechanism of geckos, structural color of a butterfly wing, anti-reflection of the moth eyes, mechanical property of the bone, and so on. Fig. 1 provides some representative biological materials from nature and their selected functions followed by their detailed descriptions. This field, known as biomimetics, offers enormous potential for inspiring new capabilities for exciting materials[1]. The word "biomimetics" was coined by Otto Schmitt in the 1950s for the transfer of ideas and analogues from biology to technology[2], and was first appeared in Webster's dictionary in 1974 and defined as 'the study of the formation, structure or function of biologically produced substances and materials (as enzymes or silk) and biological mechanisms and processes (as protein synthesis or photosynthesis) especially for the purpose of synthesizing similar products by artificial mechanisms which mimic natural ones' [3]. It is defined biomimetics as a science of systems which has some function copied from nature, or which represents characteristics of natural systems or their analogues [4] till now.

The approach of bio-inspired design has been utilized for thousands of years. It began with mimicking the motions or functions of animals to improve the capability of human beings, and then gradually shifted to the creation of novel materials and devices. For example, people learned how to fly from birds, and submarines were created by learning from fish. However, biological materials are highly organized from the molecular to the nanoscale, microscale and macroscale, often in a hierarchical manner with intricate nanoarchitecture that ultimately makes up a myriad of different functional elements. Structural biomimetic or bio-inspired materials refer to the materials which imitate the structures or the characteristics of the biological materials. In recent years, a great deal of work has been devoted to fabricating multiscale structures with functional properties through the biomimetic or bio-inspired approach. Table 1 lists the advantages and disadvantages of some common methods of fabricating biomimetic or bio-inspired structure or materials as well as the corresponding biological materials. As a versatile and cost-effective nanofabrication technology, the fascinating morphologies and structures fabricated by electrospinning demonstrate the excellent prospects of this method for construction of biomimetic structures.

In this review, we mainly summarize some living organisms with multilevel hierarchical micro-nano structures including plant-based soft tissue bio-materials, animal-based soft tissue bio-materials and animal-based hard tissue bio-materials (e.g., the lotus leaf, moth eye, bone, etc.) with corresponding special functions (e.g., superhydrophobicity, anti-reflectivity and toughness). Particularly, the artificial biomimetic architectures of the aforementioned structures via electrospinning, as well as the prospects and challenges in the future, have also been proposed.

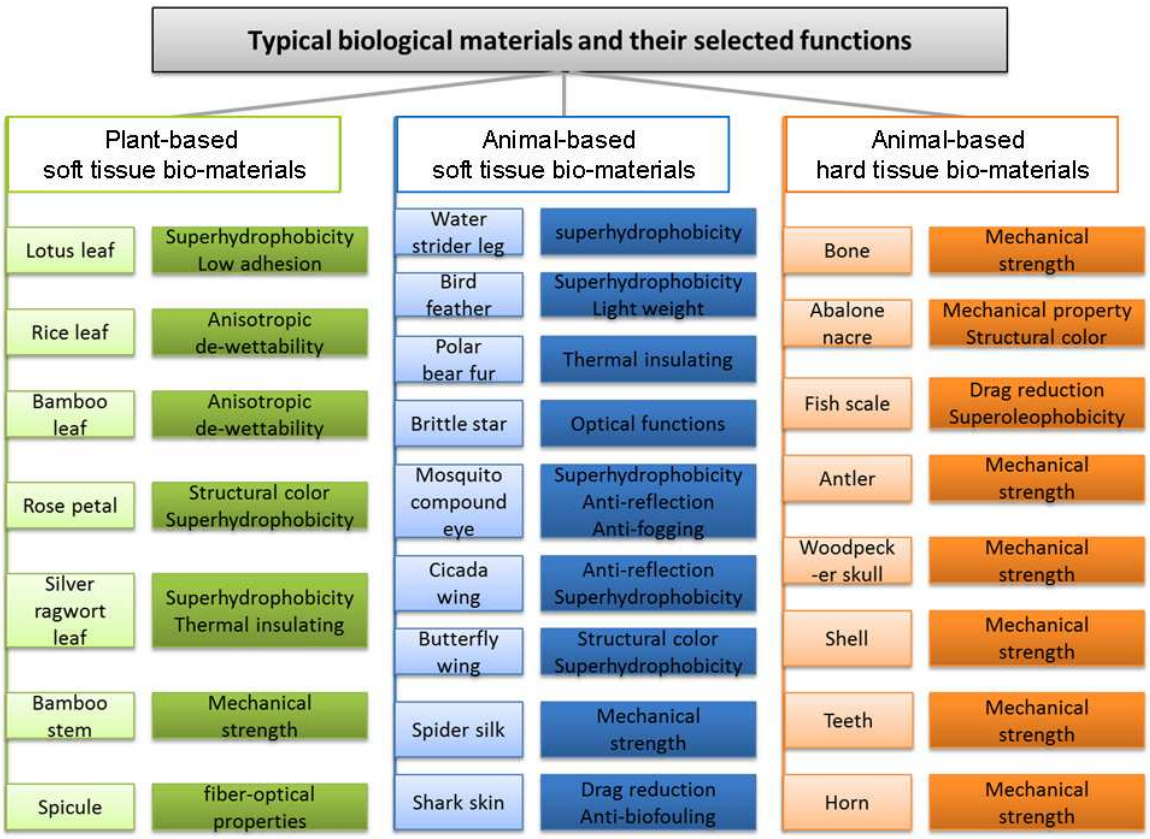

Figure 1. Typical biological materials and their selected functions.

Table 1 Common methods of fabricating bio-inspired materials

Methods	Advantages	Disadvantages	Biologic materials	Ref.
Electrodeposition	Simple and inexpensive; Effective and versatile for fabricating a variety of structures; Easy to control the size, shape, and structural properties	A mold or template of porous membrane is needed; Three electrodes; Hard control of membrane pore diameters, interpore distances, and thicknesses; Crack formation	Lotus leaf; Cauliflower; Rice leaf; Gecko's foot; Shark skin	5-9
Chemical vapor deposition	Uniform film thickness; Independent from substrate forms/shapes; Relatively high efficiency; Easily controllable; Mass productions	Required heterogeneous reactions; Complex equipment; High temperature; Volatile metallic chlorides and fluorides as their main materials; Expensive	Lotus leaf; Morpho butterfly wing; Gecko's foot; Moth eye	10-13
Lithography	High similarity; Simple equipment; Low cost; High throughput; From nano to larger structures	A mold or template is needed; Adhesion between resist material and template; A residue layer left; Limited	Lotus leaf; Morpho butterfly wing; Shark skin;	14-17

		capability in producing complex 3D structures;	Moth eye	
Templating/ Molding/Casting	High yield; High similarity; Perfect performance	Complex process; A mold or template is needed; Microscale	Lotus leaf; Morpho butterfly wing; Gecko's foot; Rose petal; Rice leaf; Moth eyes; Cicada wings	8,18-23
Plasma/laser treatment	High similarity; High yield; Mass replication of tightly controlled features	Low efficiency; High cost; Microscale;	Lotus leaf; Gecko's foot	24-26
Layer-by-layer technique	Ease of preparation; Versatility; Fine control over the materials' structure; Robustness of products; Nanoscale	Lack of precise control; Less straight forward for the Preparation; Lack of surface roughness	Lotus leaf; Morpho butterfly wing; Nacre; Water striders leg	27-30
Self-assembly	Extremely high efficiency; Structural control; Reproducibility Controllability; Defect tolerance	Lack of better or more precise controllability; Need for more control of the entire morphology, the symmetry	Morpho butterfly wing; Moth eye; Nacre	31-33
Sol-gel process	Low cost; Molecular-scale homogeneity; Fairly simple controllable; Outstanding performances	Hot solution; Difficult to control regular surface pattern; use a large amount of solvent	Lotus leaf; Morpho butterfly wing; Moth-eye; Gecko's foot	34-37
Biomineralization	Simple process; High yield; Perfect performance	Low similarity; Microcscale	Bone; Nacre; Shell; Teeth	38-41
Genetic recombinant	Almost same structure, property; Mass production	High workload; High cost; Complex process	Spider silk	42-44
Electrospinning	Different nanofiber assembly; Various of fiber structures; Superior performance	Lack of precise design; Instability of product morphology and performance	Lotus leaf; Rice leaf	45 46

2. Electrospinning fundamentals

Electrospinning (or electrostatic spinning), which was originated from electrospraying, was first observed in 1882 by Rayleigh[47], studied in detail by Zeleny [48], and patented by Formhals in 1934 [49]. The work of Taylor on electrically driven jets has laid the groundwork for electrospinning [50-52]. As shown in Fig.2a, a typical electrospinning setup is composed of three basic elements: a high voltage power supply, a syringe needle and a grounded target (usually a metal screen, plate, or rotating mandrel). One electrode of the high voltage power supply

is connected with the spinneret containing the spinning solution and the other attached to the collector which is usually grounded[53]. During electrospinning, a solution is first fed through a spinneret and a high voltage is applied to the solution at a critical voltage (typically more than 5 kV). When the electric force is larger than the solution's surface tension, a jet would erupt from the tip of the spinneret. Although the jet is stable near to the tip of the spinneret, it soon enters a bending instability stage with further stretching of the solution jet under the electrostatic forces in the solution as the solvent evaporates (Fig.2b). Finally, the continuous as-spun fibers are deposited, commonly as a 2D nonwoven web, on the collector.

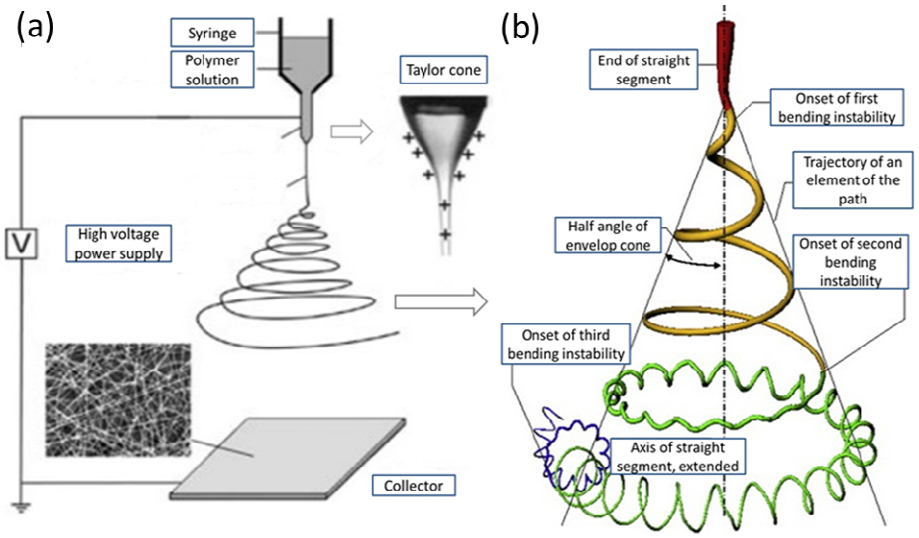

Figure 2. (a) Schematic illustration of a typical basic electrospinning setup, the Taylor cone, and a SEM image of electrospun nanofibers. (b) A diagram that shows the prototypical instantaneous position of the path of an electrospinning jet that contained three successive electrical bending instabilities. (a) Reprinted with permission from [54]. Copyright 2004 WILEY-VCH Verlag GmbH & Co. KGaA, Weinheim. (b) Reprinted with permission from[55]. Copyright 2008 Elsevier.

The electrospinning process is solely governed by many parameters, classified broadly into solution parameters (including viscosity, conductivity, molecular weight, and surface tension), process parameters (e.g., applied electric field, tip to collector distance, feeding or flow rate), and ambient parameters (e.g., humidity and temperature of the surrounding)[56]. Each of these parameters significantly affects the resultant fibers' morphology, and by proper manipulation of these parameters we can get micro/nanofibers with desired morphology and diameters [57]. For instance, the polymer solution must have a concentration high enough to cause polymer entanglements yet not so high that the viscosity prevents polymer motion induced by the electric field. The solution must also have a surface tension low enough, a charge density high enough, and a viscosity high enough to prevent the jet from collapsing into droplets before the solvent has evaporated. Morphological changes can occur upon decreasing the distance between the syringe needle and the substrate. Increasing the distance or decreasing the electrical field decreases the bead density, regardless of the concentration of the polymer in the solution. Applied fields can, moreover, influence the morphology in periodic ways, creating a variety of new shapes on the surface. Important electrospinning parameters which control fabricated fiber properties are to be highlighted here such as: applied voltage, tip to collector distance, flow rate, polymer concentration, solvent dielectric constant and, collector spinning rate, which have been summarized and reviewed previously [54,56-58].

As an unique spinning technique, electrospinning uses electrostatic forces to produce fine fibers from polymer

solutions or melts and the fibers thus produced have a thinner diameter (from nanometer to micrometer) and a larger surface area than those obtained from conventional spinning processes (wet spinning, dry spinning, melt spinning, gel spinning)[59,60]. Nevertheless, the random orientation of fibrous mats fabricated by conventional electrospinning may limit the potential applications of electrospun fibers. Therefore, to overcome various limitations of the typical electrospinning setup and to further the performance of the electrospun products, researchers have come out with other modifications to the setup with well- modified and designed fiber generators, collector, auxiliary electrodes and applied voltage[61-65], and so on. And various materials such as polymers, composites, ceramics and semiconductors, etc., can be fabricated as different morphologies and structures (e.g., random oriented, aligned as well as patterned, spider-web-like nanofiber/net structures) by controlling the aforementioned techniques[66-69]. Furthermore, through regulating the processing parameters or designing appropriate spinnerets and auxiliary electrodes, individual nanofiber structure (e.g., bead-on-string, ribbon-like, core-sheath or hollow, multichannel tubular, nanowire-in-microtube, multi-core, cable-like, porous and branched structure) can also be generated[70,71], which will be of significance for broadening the application fields of electrospinning.

3. Design of plant-based soft tissue bio-materials

3.1. Lotus leaf

Since Barthlott and Neinhuisfirstly revealed the superhydrophobicity of lotus leaves in 1997 [72], the self-cleaning lotus leaf has been among the most well-known studied species [73-76] which attracts numerous researchers to be engaged in fabricating superhydrophobic surface, and a variety of methods have been emerged for constructing the superhydrophobic surfaces, such as electrohydrodynamics[77], templation[19], electrodeposition[78], nanoimprint lithography[79], laser ablation[80], and sol-gel[81]. Raindrops are almost spherical on lotus leaf surface and able to roll off easily, which is usually referred to as the well-documented “lotus effect” [82,83] (Fig.3a). The lotus leaf exhibits a high water contact angle (WCA) of around 160° [84] and a small sliding angle (SA) of about 2° [83]. Investigations showed that this unique property is caused by the surface micrometer sized papillae (Fig.3b). However, detailed scanning electron microscopy (SEM) images of lotus leaves indicate that the surface of the lotus leaf is textured with 3~10 μm size protrusions and valleys uniformly, which are decorated with 70~100 nm sized particles of a hydrophobic wax-like material [85] (Fig.3c). The combination of these unique micro- and nanoscale hierarchical surface structures and hydrophobic wax-like material is believed to be attributed to the superhydrophobicity [86].

Heng et al.[45] prepared a hexaphenylsilole (HPS)/polymethyl methacrylate composite film with a lotus leaf like structure by a simple electrospinning method which shows high stability and excellent sensitivity for the metal ions Fe^{3+} and Hg^{2+}. The membrane mimicked the lotus leaf shape rather than lotus-leaf-like structure, even though it showed a WCA of about 115° (Fig.3d). Nevertheless, a lotus leaf-like structure could obtain by depositing droplets or collecting beads on a fiber membrane. Yoon et al.[87] described the fabrication of a biomimically designed surface, which is similar to that of the superhydrophobic lotus leaf. They achieved a superhydrophobic surface exhibiting a micron-sized pyramid structure consisting of accumulated electrosprayed poly (ε-caprolactone) (PCL) droplets on the surface of electrospun PCL nanofibres (Fig.3e). Through this process, they obtained a superhydrophobic surface having a WCA greater than 172° and a sliding angle of 14°. Lee et al.[88] prepared lotus-leaf-like nanofibrous surfaces by electrospinning hydrophobic poly (vinylidene fluoride) (PVDF). Micron-sized beads were introduced to the electrospun PVDF mats, resulting in enhanced hydrophobicity of the electrospun mats (Fig.3f). The addition of a

small amount of acetic acid to the polymer solution effectively improved the bead-on-string morphology of the electrospun mats, and led to a higher WCA. The electrospun PVDF fibrous mat showed a maximum WCA of 148.5° due to the appropriate surface roughness. When mimics lotus leaf, there still is randomness in the control of morphology of droplets and size of the beads, which would lead to the instability for the superhydrophobicity of the fabricated hydrophobic material. It was demonstrated by Shiratori et al. that lotus leaf structure can be mimicked by creating a rough surface texture through heating polyelectrolyte multilayer films containing silica nanoparticles via LBL assembly[89]. Thus, Ma et al.[90] introduced the LBL technique into the electrospun fibers to construct superhydrophobic surfaces whose contact angle (CA) did not change as the droplet evaporated, indicating a stable superhydrophobicity with almost zero contact-angle hysteresis[90] (Fig.3g). The average CA for the treated fiber mat was 168°, which could be attributed to the high density of nanoparticles decorated on the surface of treated fibers.

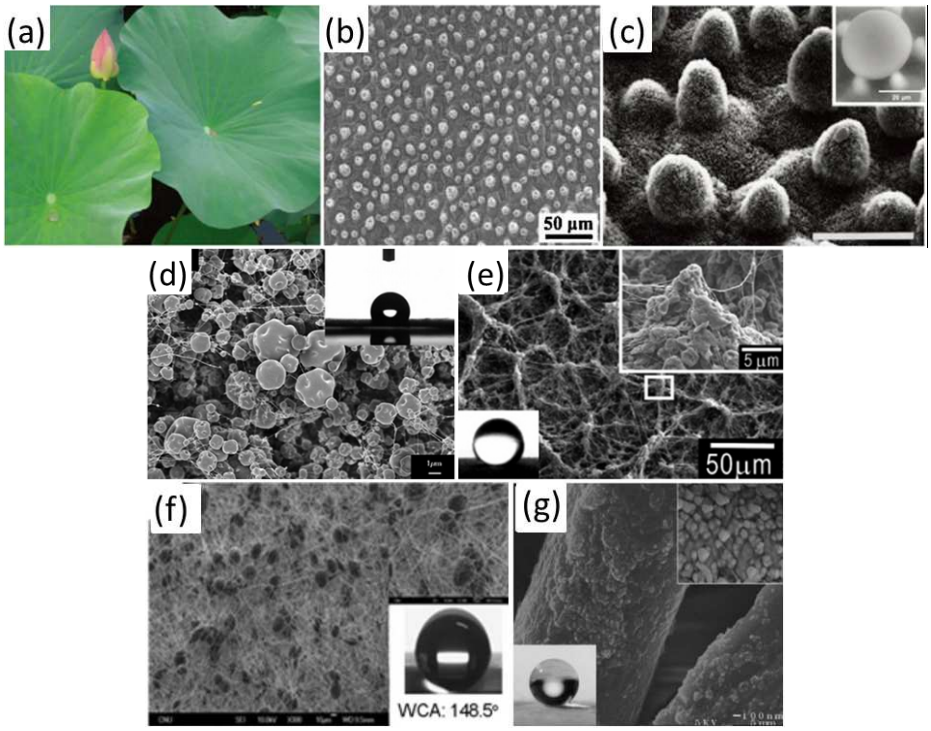

Figure 3. (a) Lotus leaves show self-cleaning properties, note that dust is accumulated in the water droplet at the center of the leaves. SEM images of surface structures on the lotus leaf with (b) low and (c) high magnifications. The scale bar in (b) represents 50 μm; (c) represents 20 μm. (d) SEM image of electrospun film; insert: Photograph of water droplet shape on the electrospun film with a WCA of (115±2.6) °. (e) Surface consisting of accumulated PCL droplets and fibers sprayed during 2 h. (f) FE-SEM images of the electrospun PVDF nanofibers with tetrabutylammonium chloride in the polymer solution. The inset picture indicates the CA of water droplet. (g) SEM image of electrospun nylon fibers after silica nanoparticle and trichlorosilane treatment.

(a) and (c) Reprinted with permission from[91]. Copyright 2011 Nano Today. (b) Reprinted with permission from[92]. Copyright 2011 Elsevier. (d) Reprinted with permission from [45]. Copyright 2008 WILEY-VCH Verlag GmbH & Co. KGaA, Weinheim. (e) Reprinted with permission from[87]. Copyright 2010 Macromolecular Rapid Communications. (f) Reprinted with permission from[88]. Copyright 2013 The Korean Fiber Society and Springer Science + Business Media Dordrecht. (g) Reprinted with permission from[90]. Copyright 2007 WILEY-VCH Verlag GmbH & Co. KGaA, Weinheim.

3.2. Silver ragwort leaf

The silver ragwort uses of fiber-like surface structure to realize the repellent of water and the properties of self-cleaning[85] (Fig.4a).It is one of the examples that have superhydrophobic leaves with WCA of about 147° [93]. By

examining the leaf with a SEM, it can be observed that the leaf is densely covered by many curved fibers with diameters around 6μm (Fig.4b). These fibers are trichomes with unicellular or multicellular structures arising from the epidermal tissues. Moreover, the secondary structures, numerous grooves with diameters around 200 nm, are found along the fiber axis (Fig.4c). The surface of a silver ragwort leaf shows a hierarchical micro- and nanostructure which is essential for achieving a high hydrophobicity[94].

As poly (vinylidene fluoride-co-hexafluoropropylene) (PVDF-HFP) is a hydrophobic polymer[95], its wettability can be turned with change in surface design or topography. In terms of pure electrospinning PVDF-HFP membrane, the as-fabricated fiber was smooth and the membrane showed a near superhydrophobicity with WCA of about 120° [96]. Lee et al.[97] prepared electrospun PVDF-HFP fibrous membranes with plasma treatment. Herein, Ar plasma was used to wrinkle the surface of the fibrous membrane, which transformed it to a superhydrophilic surface (Fig.4d) and the membrane surface CA could be increased to 150°. Except for the hydrophobic polymer, a well-known material with low surface energy is polystyrene (PS), which can be used to make superhydrophobic surfaces[98]. Kang et al.[99] obtained PS fibers from the highly viscous solution of PS in DMF exhibited an intriguing surface morphology with numerous protuberances and wrinkles which imitated the structures of lotus leaf and silver ragwort leaf (Fig.4e). The CA measurements indicated that the electrospun fibrous membranes were superhydrophobic with a WCA of 154.2±0.7°. This superhydrophobicity was attributed to the combined effects of the regular nanostructural protuberant and wrinkled morphology formed on the surfaces of the individual fibers during electrospinning and the microstructural surface roughness of the electrospun membrane itself. Lin et al.[100] demonstrated the fabrication of PS superhydrophobic fibrous mats in the presence of silica nanoparticles which imitated the structures of lotus leaf and silver ragwort leaf, too (Fig.4f). The resultant electrospun fiber surfaces showed a stable superhydrophobicity with a WCA as high as 157.2° when containing 14.3 wt. % silica nanoparticles.

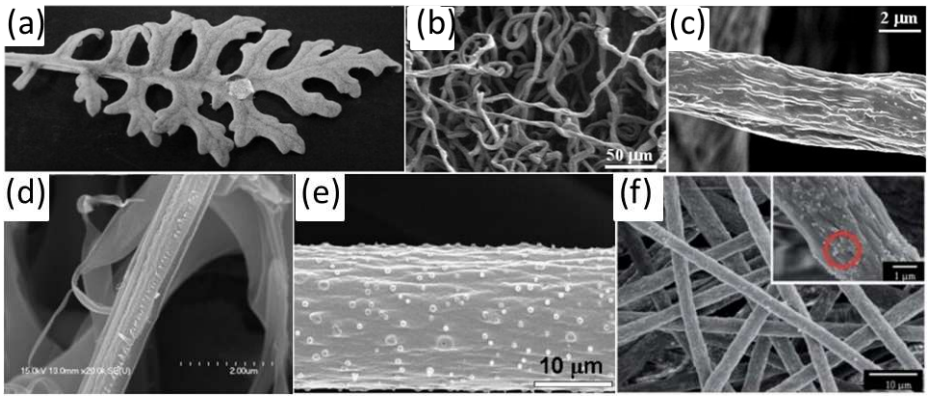

Figure 4. (a) Photograph of a water droplet on a silver ragwort leaf. (b), (c) SEM images of the leaf at different magnifications. (d) FE-SEM images of PS fibers electrospun from DMF with 14.3 wt. % contents of silica. (e) FESEM images of electrospun PS fibers from 35 wt. % solution in DMF. (f) Hollow fibers by carbothermal reduction and nitridation of electrospun composite fibers.
(a-c) Reprinted with permission from [93]. Copyright 2006 Nanotechnology. (d) Reprinted with permission from [97]. Copyright 2013 Corresponding author, Pusan National University, Korea. (e) Reprinted with permission from [99]. Copyright 2008 Elsevier. (f) Reprinted with permission from [100]. Copyright 2011 Royal Society of Chemistry.

Besides its high hydrophobicity, scientist also found white color of silver ragwort leaf is not due to any dye substance but is related to trichomes on the plant surface[101]. The plant is densely covered with a layer of woven hollow fibers with diameters of about 6 μm. These hollow fibers are responsible for the white color of the plant. One

of the characteristics of the trichomes is that it is highly resistant to strong irradiation of sunlight and therefore they protect the plants from damage due to strong sunlight [94]. In order to artificially fabricate the surface of silver ragwort and endow it with both superhydrophobicity and light shielding ability, Gu et al.[94] prepared electrospun PS membrane which exhibited a similar color as the white-color plants (Fig.5a). The CA tested by applying water drops onto the surface can be as large as 156° and light-shielding ability checked by monitoring the temperature change of the substrates under an irradiation of strong light showed well (Fig.5b). However, to mimic the hollow structure densely covered with a layer of woven fibers, Ge and his coworkers[102] gave us a clue that they fabricated hollow multilayered fibers by the combination of the electrostatic LBL assembly and electrospinning methods (Fig.5c). What they obtained was a hollow multilayered polyelectrolyte (PE) nanofiber whose Young's modulus was about 21.6GPa which is much larger than that for most synthetic organic fibers and similar to that of human bone fibers. Consequently, it is possible to prepare a hollow multilayered fiber containing both superhydrophobicity and light shielding ability if appropriate polymers are employed. According to the method, a silver ragwort leaf-like structure can be realized. It will also have toughness.

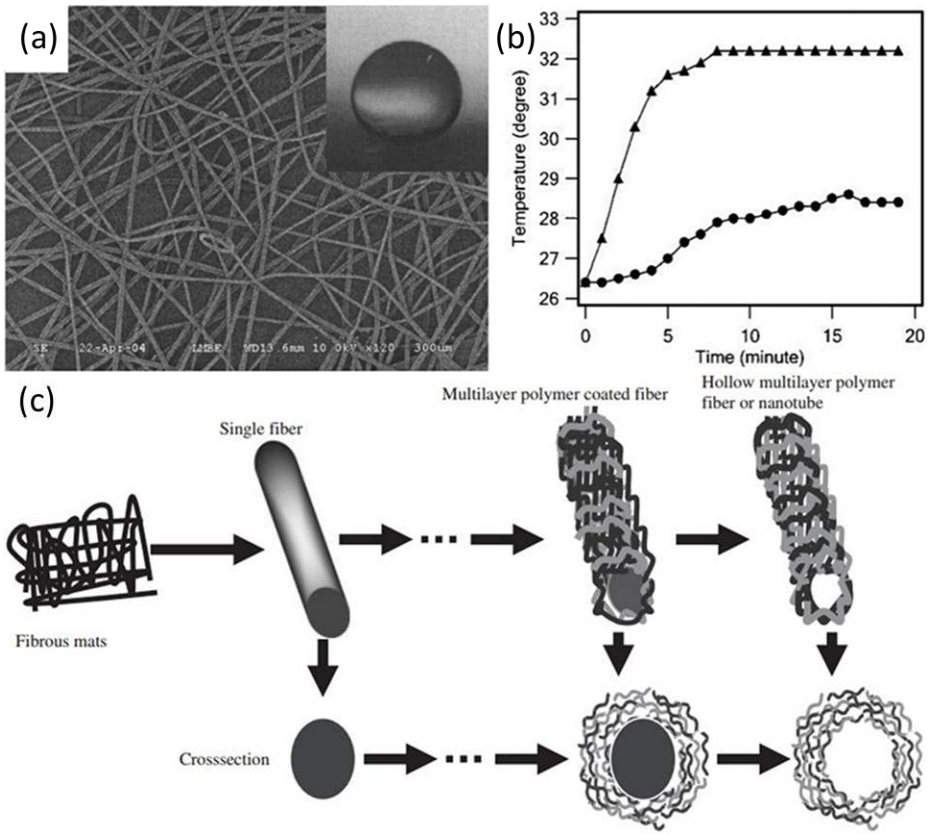

Figure 5. (a) trichome like fibers. (b) Temperature changes of the copper plates with (circle) and without (triangle) coating under an irradiation of light. (c) Schematic diagram illustrating the fabrication of hollow multilayer polyelectrolyte nanofiber via LBL coating and removal of the template.

(a-b) Reprinted with permission from [94]. Copyright 2005 Applied Physics Letters. (c) Reprinted with permission from [102]. Copyright 2007 Japan Society of Applied Physics.

3.3. Rice leaf

The rice leaves, which possess a hierarchical structure similar to the lotus leaves, show superhydrophobicity with a WCA of 157±2°. Rice leaves exhibit the ability to directionally control the motion of water microdroplets,

namely anisotropic wetting. The sliding angles of these two directions are 3~5° and 9~15°, respectively[85] (Fig.6b). Due to this special structural surface, increasing attention has been paid to anisotropic wettability[103-105]. Numerous artificial surfaces with wetting anisotropy inspired by the hierarchical structures of rice leaf surfaces have been developed using various methods, including micromolding[106], nanoimprint lithograph[107], photo lithography[108], and LBL assembly[109]. Scanning electron microscope (SEM) image of a rice leaf revealed the surface of the rice leaf consists of dual-size structures: micrometer-scale papilla and nanostructures (Fig.6a). However, there is a special kind of microstructure: sub-millimeter-scale groove arrays (Fig.6c). The width and depth of these arrays reach up to 200 and 45 μm (Fig.6d), respectively. There were also full papilla structures of micrometer-scale, with heights and widths of approximately 3~5 and 5~8 μm, respectively[110]. There is a three-level geometrical structure (macro/micro/nano) on the surface of the rice leaf (Fig.6e). The micro- and nano-hierarchical structures of the rice leaf are crucial to superhydrophobicity (Cassie's state), while the third-level microgroove arrays provide an energy barrier to travel in orthogonal directions and contribute to the anisotropic sliding phenomenon[108]. It is also observed there exist nanoscale waxes densely dispersed over the surface, resulting in a superhydrophobic surface similar to that of the lotus leaf[109] (Fig.6f).

When relatively small diameter beads were introduced to fiber film, hydrophobicity was demonstrated to increase monotonically and the amount of bead will truly influence the value of the CA[111,112]. To mimic the rice leaves, anisotropic surfaces can be made by simply aligning electrospun nanofibers by careful design of the fiber collector together with beads. Ma et al.[46] combined electrospinning and initiated chemical vapor deposition (iCVD) to produce superhydrophobic fabrics, where electrospinning generated surface roughness and iCVD reduced surface energy. A polyacrylonitrile (PAN) mat comprising bead-on string aligned fibers, with 100 nm average fiber size and 2 μm bead sizes, was first electrospun between parallel electrodes and then coated by iCVD with a 70 nm conformal layer of polymerized perfluoroalkyl ethyl methacrylate (PPFEMA). When the fiber is fixed on the slide, gaps between fiber and glass slide formed the grooves, and fiber beads made up the papilla, similar to those of rice leaf. The surface exhibited superhydrophobic behavior with a WCA of 153° and a threshold sliding angle of 8° in the direction parallel to fiber axis, and a non-superhydrophobic behavior (WCA of 119°) in the perpendicular direction.

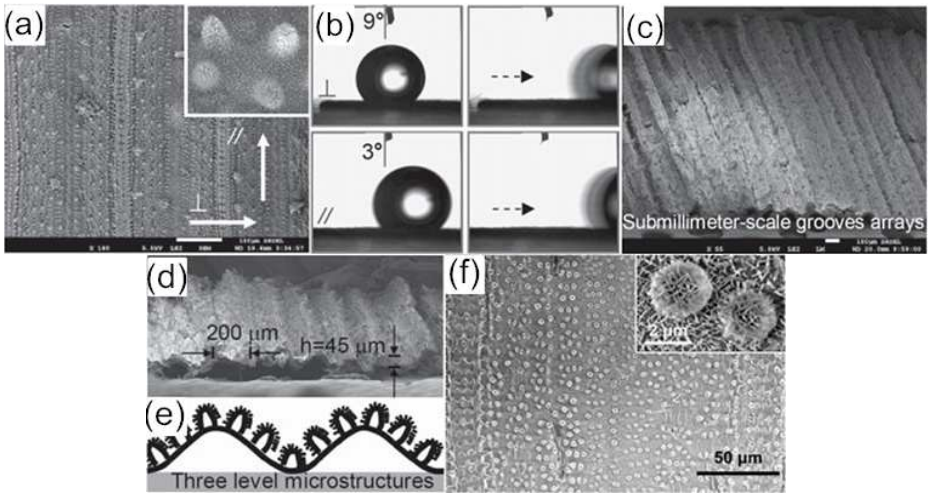

Figure 6. (a) Top-view SEM image of the rice leaf. The inset is the magnified image of dual-size structures; micrometer-scale papilla and nanostructures. (b) The anisotropic sliding property of the rice leaf. (c) 60°-tilted-view SEM image of the rice leaf. (d) Cross-sectional SEM image of the macro- grooves; width = 200 μm and height = 45μm. (e) Proposed three-level model of the rice leaf. (f) Image of the upper surface of the rice leaf, he inset shows a magnified image of the papillae covered by wax.

(a-e) Reprinted with permission from [108]. Copyright 2011 WILEY-VCH Verlag GmbH & Co. KGaA, Weinheim. (f) Reprinted with

permission from [109]. Copyright 2013 WILEY-VCH Verlag GmbH & Co. KGaA, Weinheim.

4. Design of animal-based soft tissue bio-materials

4.1. Water strider legs

Water striders are a type of insect with the remarkable ability to stand effortlessly and slide and jump promptly on water surfaces using their water-resistant legs [113] (Fig.7a). Locomotion on the surface of water of this fascinating animal has been the subject of numerous studies[113-117]. Scanning electronic micrographs (SEM) showed that the supporting legs of water strider are superhydrophobic, as the result of the cooperation of the uniquely hierarchical surface structure of needle-shaped micro-setae with elaborate nano-grooves and the covered hydrophobic wax layer. The diameters of setae ranges from 3 mm down to several hundred nanometers and most are roughly 50 μm in length and arranged at an inclined angle of about 20° from the surface of leg[118] (Fig.7b). Until a dimple of about 4.3 mm depth is formed, water strider's legs do not penetrate into the water surface. The maximal force which supports each leg of water strider is about 15 times the total its body weight (152 dyn) (Fig.7c) [113,119]. This striking repellent force is attributed to the superhydrophobicity on the legs, which is verified by a static WCA of about 167.6±4.4° [83].

To fabricate an artificial water strider, Wu et al.[120] utilized electrospun nanofiber wrapped silver wires where fibers formed a porous web around the silver wire core (Fig. 7e). When floating on the water, the porous web prevents the legs from becoming wet (Fig. 7d). Moreover, the maximal supporting force of man-made leg coated with the superhydrophobic films increases at least 2.4 times compared with the bare hydrophobic copper leg. The artificial water strider only mimicked the superhydrophobicity of the real one and the special structure of the leg surface was ignored. Xue et al.[121] reported the first electrospinning of a Polyhedral oligomeric silsesquioxanes (POSS), polymethylmethacrylate (PMMA) copolymer into uniform fibers that can form a highly superhydrophobic membrane with a WCA＞160° and SA as low as 6.3°. More interestingly, the bead-free electrospun fibers showed a nanofibrillated structure. These features have not been reported for any electrospun fibers. The photo image given in Fig.7 (f) shows a secondary structure formed on the fiber surface, which is similar to the seta of a water strider's leg (Fig.7c). Such a secondary surface structure was only observed on the uniform fibers electrospun from 5~10 wt. % polymer solutions.

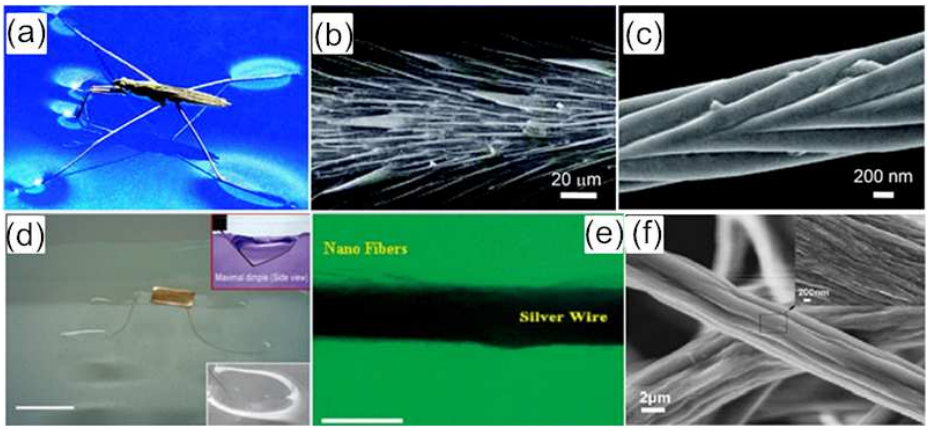

Figure 7. (a) Photograph of a water strider standing on the water surfaces. (b) Numerous oriented microscale setae and (c) nanoscale grooved structures on a seta. (d) A model man-made water strider standing on the water surface. A copper strip with a mass of 0.5 g was carried. Upper inset is the side view of the strider leg walking across the water surface. Lower inset notes the deformation of the surface around the legs. Scale bar: 1 cm. (e) Optical microscopy image of one leg of the miniature water strider showing porous nanofibers

coated on a silver wire. Scale bar is 200 mm. (f) The SEM examination revealed that the constituent setas consisted of uniform fibril bundles.

(a-c) Reprinted with permission from [122]. Copyright 2007 American Chemical Society. (d-e) Reprinted with permission from [120]. Copyright 2008 Royal Society of Chemistry. (f) Reprinted with permission from [121]. Copyright 2009 Royal Society of Chemistry.

4.2. Feather

Feathers also have attracted a lot of attention due to their high hydrophobicity [123-125]. The microscopic structure of feathers appears to conform closely to the requirements for optimal water repellency. Fig.8 (a) shows an optical picture of a piece of duck feather, indicating that duck feathers are highly ordered and have hierarchical branched structures. Fig.8 (b) shows that duck feathers are composed of branches with different dimensions, including micro-sized backbones (rachis), trunks and barbules. And the branch is composed of micro-sized tomenta which has nanosized grooves and protuberances (Fig.8c). SEM images reveal that duck feathers have multi-scale texture and the water repellency of the bird feather in general is attributed to the trapped air space in it, forming an air cushion at the feather–water interface thereby keeping the feather from being wet. According to the principles of superhydrophobicity, increasing of the surface roughness of a solid surface can result in increasing of the water contact angle which ranges from 100°~140°[123].

To mimic the branched surface of the bird feather, Wu et al.[126] fabricated branched poly (vinyl alcohol) (PVA) nanofibers by coaxial electrospinning of two-liquids under an alternating magnetic field in a facile manner (Fig.8d). The resultant branched structure showed that both the PVA nanofiber trunks with diameter of 100~200 nm and the PVA nanofiber branches with diameter of 10~30 nm were formed in a single step (Fig.8e). However it did not show any water repellency. To obtained a similar branched structure as well as superhydrophobicity, Wu et al.[120] produced a feather-shaped radiating poly (vinyl butyral) (PVB) nanofiber pattern by collecting fibers between a metal needle and a straight strip (Fig.8f). Obviously, both droplets have a streamlined shape indicating a similar wetting anisotropy as the feather (Fig.8g and h). While Wu et al.[120] shows us the superhydrophobic branched structure, the structure exposes to us the embarrassment at the same time, because it lacks mimcing the tomenta structure of the feather. In terms of grooves and protuberances of the mimiced feather, electrospinning combined with electrospraying can be adopted[127]. As shown in Fig.8i, well-aligned nanofiber array can be obtained on the high-speed rotator by electrospinning while nanoparticles by electrospraying simultaneously. Firstly, a highly aligned nanofiber array containing nanoparticles is collected at the high-speed rotator. Then remove it from the rotator and set it over two fix point, a fiber bundle is possible to be created by this proper means[128] (Fig.8j). Thus a manmade feather-like structure is got where nanoparticles act as protuberances and valleys act as grooves. (Fig.8k). We would find that water will be aligned along the direction of grooves, and groove depth, groove width as well as particle size will be truly influential on water morphology, thus to the WCA. By employing proper polymers (e.g., PVDF, POSS), this artificial feather will show superhydrophobicity.

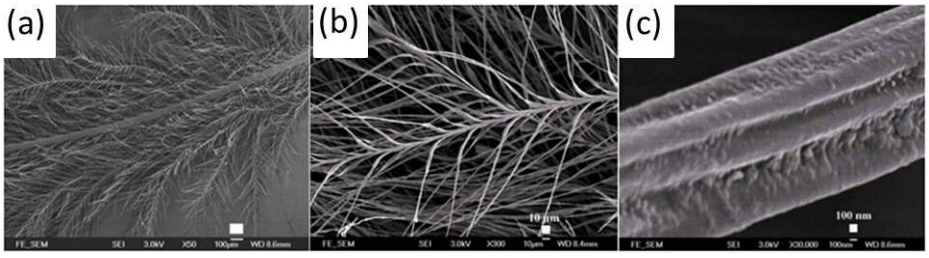

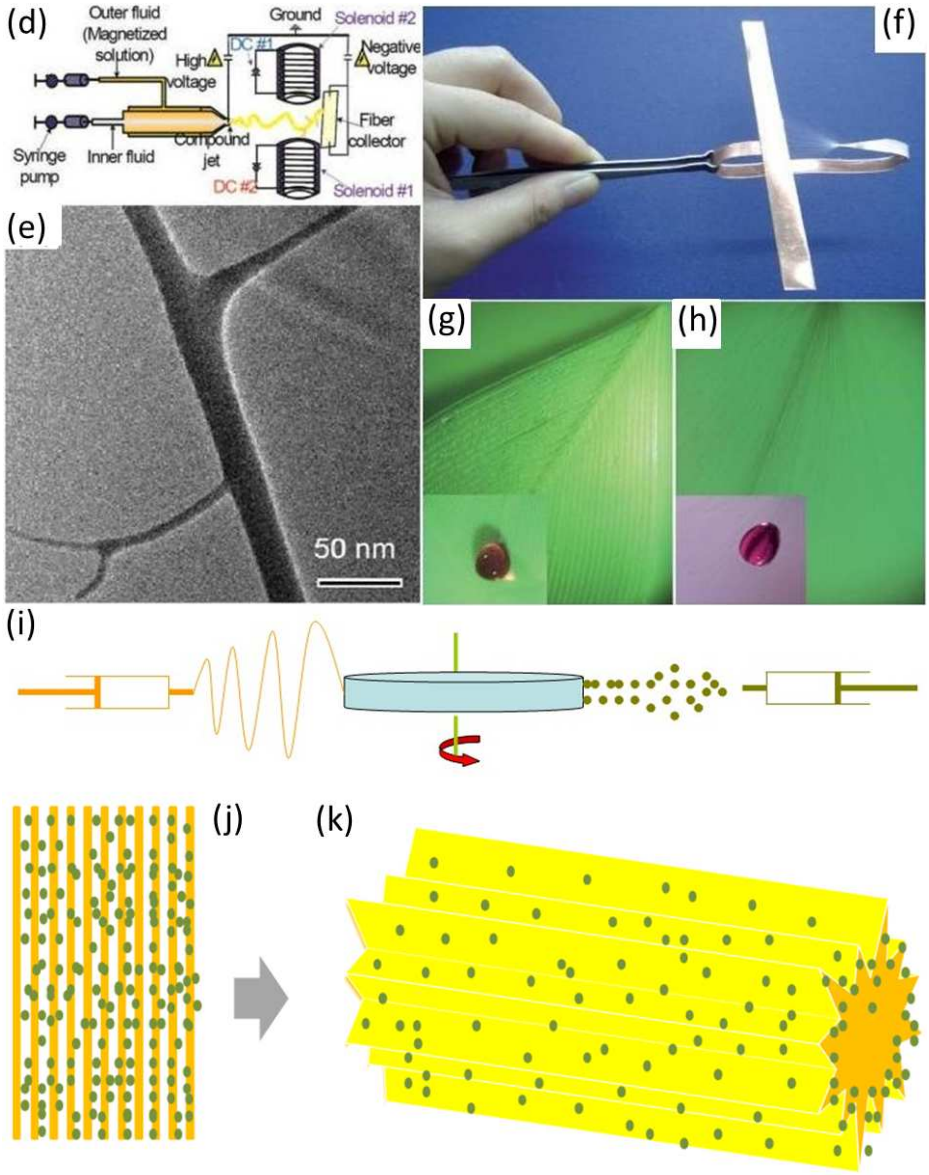

Figure 8. (a) FE-SEM image showing hierarchical structure of duck feather (scale bar, 100 mm). (b) FE-SEM image of tomenta of a duck feather (scale bar, 100 nm). (c) Schematic illustration of electrospinning technique for forming branched nanofibers. (d) TEM images of hyperbranched nanofibers. (e) Digital photograph of fan-shaped radiating nanofiber pattern collected by a spiculate copper needle perpendicular to a rectilinear copper strip. (f) and (g): A water droplet set on the surface of (f) goose leaf, (g) Fan-shaped radiating nanofiber pattern. (i) Schematic illustration of the electrospinning/electrospraying setup. (j) nanofiber array containing nanoparticles. (k) artificial feather.

(a-c) Reprinted with permission from[123] . Copyright 2008 IOP Publishing. (d-e) Reprinted with permission from [126]. Copyright 2012 Wiley Periodicals, Inc. (f-h) Reprinted with permission from [120]. Copyright 2008 Royal Society of Chemistry.

What's more, envied by scientists, delicate hollow structures have been adopted by feathers of many birds with multichannel inner structure (Fig.9a). It is the structure that could reduce weight by increasing friction with air and serve as heat-shields from intense solar radiation[129,130]. Multichannel structures may possess considerable advantages such as independent addressable channels, better mechanical stability, unique thermal properties and larger surface-to-volume area which might be promising candidates for a wide range of applications such as bionic super lightweight, thermo-insulated textiles[131]. More recently, inspired by multi-channel inner structures of bird feathers,

Zhao et al.[132] developed a multi-fluidic compound-jet electrospinning technique to fabricate biomimetic hierarchical multi-channel microtubes (Fig.9b and c). Such nanofibers should be of novel and improved properties that do not exist in each component. It is a promising candidate for a wide range of applications, such as for bio-mimic super-lightweight thermoinsulated textiles.

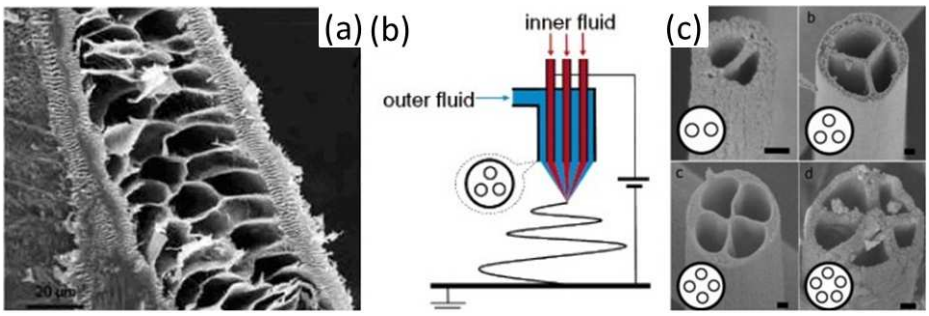

Figure 9. (a) Multichannel inner structure of feather barb. (b) Schematic illustration of the three-channel tube fabrication system. (c) SEM images of multichannel tubes with variable diameter and channel number. (a) Reprinted with permission from[133]. Copyright 2008 Elsevier. (b-c) Reprinted with permission from[132]. Copyright 2007 American Chemical Society.

4.3. Butterfly wings

It was pointed out that Morpho butterflies produce rather remarkable colors, also known as structural colors, providing a striking example of pattern formation in biological systems[134,135]. The origin of the brilliant blue color of Morpho butterflies wing has been studied by so many researchers that a variety of mechanisms appeared, such as blue light reflection[136], optical interference[137], light diffraction[138], light scattering[139] and photonic crystal effect[140]. Because of the striking iridescent color, methods of replicating butterfly wing appeared, for example atomic layer deposition[141], molding lithography[142], sol-gel deposition[143], nanoimprint lithography[144]. It is revealed that the hierarchical photonic structures of the wing scales play a critical role for the formation of its beautiful color of Morpho wings (Fig.10a) [145]. The wing is made of quite small scales and forms at least two layers over the wing membrane. The typical dimension of the scale is 150 μm in length and 60 μm in width. Thirty five to forty rows of lamellas align on the scale surface with almost an identical interlacing (Fig.10b). Furthermore, there are several ridging stripes (~184 nm in width and ~586 nm in clearance) on the surface of each scale (Fig.10c). The fine nanostripes are composed of multiple layers of cuticle lamellae of varying dimensions and are stacked stepwise. The lamellae are located 1.6 μm from each other and supported by cross-ribs, which dictate the interlamellae spacing and hold the lamellae 1 μm above the bottom surface of the scales. This so-called organizational color is produced by light interference, diffraction and scattering[135,141,146].

The elaborate architecture in butterfly wing is primarily based on photonic crystal structures, which all demonstrate great skill in physical manipulation of light. These structures can broaden the horizon for the design of photocatalysts[147]. Chen et al.[148] created a multilayer scattering-enhanced photoactivity where the electrospun titanium tetraisopropoxide (TTIP)/ poly (vinyl pyrrolidone) (PVP) nanofibers deposited prior to a blocking layer and a prefabricated layer. Then the multilayer sequentially was introduced onto the glass slide coated with fluorine-doped tin oxide (FTO) and finally calcinated at 450°C under air atmosphere to eliminate organic residues and to encourage the crystallization of titania. Result showed the structure has a 99% scattering and confirmed the scattering-enhanced photoactivity of the electrospun titania nanofibers to be utilized as wavelength-dependent light propagation materials. Shang et al.[149] synthesized a multicomponent oxide, Bi_2WO_6/TiO_2 as an example, with hierarchical heterostructure

successfully as a mat via electrospinning (Fig.10d). Due to the structure-property relationships, the as-prepared hierarchical heterostructure exhibited enhanced visible photocatalytic activity (photodegradation efficiency of rhodamine B reaches nearly 100% after 30 min of visible-light irradiation) and close investigation revealed that the surface area, grain size, and hierarchical heterostructure of the Bi_2WO_6/TiO_2 mat could improve the photocatalytic activities.

To fabricate a film with structural color, the fiber should be meticulously arranged in a particular way. Kuwayama et al.[150] reported that mats of electrospun fibers with a narrow distribution of diameters with wavelengths in the visible region show different structural colors depending on fiber diameter owing to the interference effect. Ma [151] demonstrated the same effect using electrospun fibers. The electrospinning fibers made from a phenylsiloxane resin/PMMA copolymer were then transferred to a glass slide and coated with PPFEMA (nominally 30 nm thick coating). The average fiber diameter before coating with PPFEMA was 1.24 μm with a standard deviation of 0.08 μm. The color observed for these fibers is believed to be the effect of Mie scattering. Based on preliminary calculations using Mie scattering model, Ma described that fibers with too small or too large sizes (diameter＜600 nm or ＞10 μm) do not have unique scattering peaks or valleys within visible wavelength and therefore structural colors.

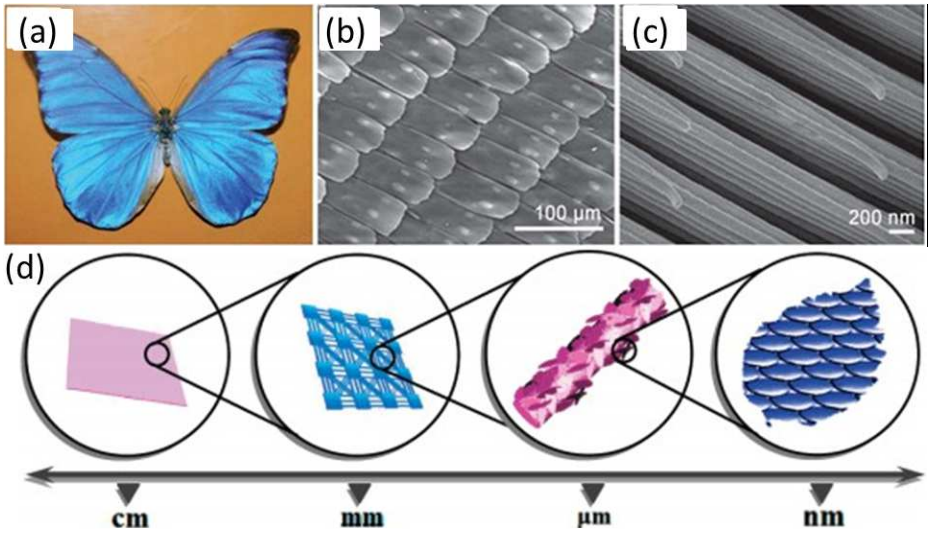

Figure 10. (a) Photograph of a Morpho. (b and c) SEM image of the hierarchical micro- and nanostructures on the surface of the butterfly wings. (b) The periodic arrangement of overlapping micro-scales on the wings and (c) fine lamella-stacking nano-stripes on the scales. (d) The Sketch Map of the Bi_2WO_6/TiO_2 Hierarchical Heterostructure. (a-c) Reprinted with permission from[145]. Copyright 2009, American Chemical Society. (d) Reprinted with permission from[149] Copyright 2012 Royal Society of Chemistry.

4.4. Corneal nipple

In the year of 1969, Bernhard, for the first time, discovered the moth cornea almost does not reflect the near-infrared light, so as to hide themselves[152]. Electron microscope studies of the corneal lenses of moths reveal that the outer surface is covered in a regular array of excessive cuticular protuberances, termed corneal nipples, typically of about 200 nm height and spacing[152,153] (Fig.11a,b and c). The nipples appeared to be arranged in domains with almost crystalline, hexagonal packing. The nipple distances were found to vary only slightly, ranging from about 180 to 240 nm, but the nipple heights varied between 0 (papilionids) and 230 nm (a nymphalid). The nipples create an interface with a gradient refractive index between that of air and the facet lens material, because their distance is

distinctly smaller than the wavelength of light[154]. Moths use hexagonal arrays of nipples as antireflection coatings to reduce reflectivity from their compound eyes, and exhibit almost perfect broadband anti-reflection properties[155]. The structure of the cornea can also increase light transmission in dark conditions, which improves the sensitivity of light vision[156]. Quite a lot of processes emerged following the first artificial moth-eye structure/film produced by interference lithography[153], like nanoimprinting[157], spin-coating technique[158], electrochemical etching[159].

TiO_2 has been widely used as antireflective coatings (ARCs) due to its matching refractive index (RI) (anatase 2.49, rutile 2.903) and low deposition cost in semiconductor detectors and photovoltaic industry[160]. Li et al.[161] fabricated particle-like TiO_2 nano-structured film coating via electrospinning. By adding a certain amount of diethanolamine (DEA) to the TiO_2 precursor solution, nanoparticles were received on a glass substrate and undergo further calcination to change to TiO_2 (Fig.11d). Its highest transmittance value was obtained at 6.0wt% DEA addition and was over 90%. One of the possible ways for antireflective coatings to function it by providing a gradient of effective optical density for light to enter a material instead of a single sudden jump. The anti-reflective property can be achieved by using monolayer coatings of sub-wavelength thickness ($\lambda/4$) with matched RI to the geometric mean of the refractive indices of the media above and below[162]. Raut et al.[163] proposed electrospinning as a technique to fabricate porous SiO_2 ARCs on large-area glass substrates. After the deposition of SiO_2 nanofibers onto a glass substrate via electrospinning, it is subsequently sintered to render sub-wavelength porous- SiO_2 anti-reflection film on the glass substrate. This resulted in formation of a dense array of a 150 nm thick, around 20 nm in diameter SiO_2 spherical nanoparticles (Fig.11e and f) ARC on the glass which has a transmittance of higher than 90%.

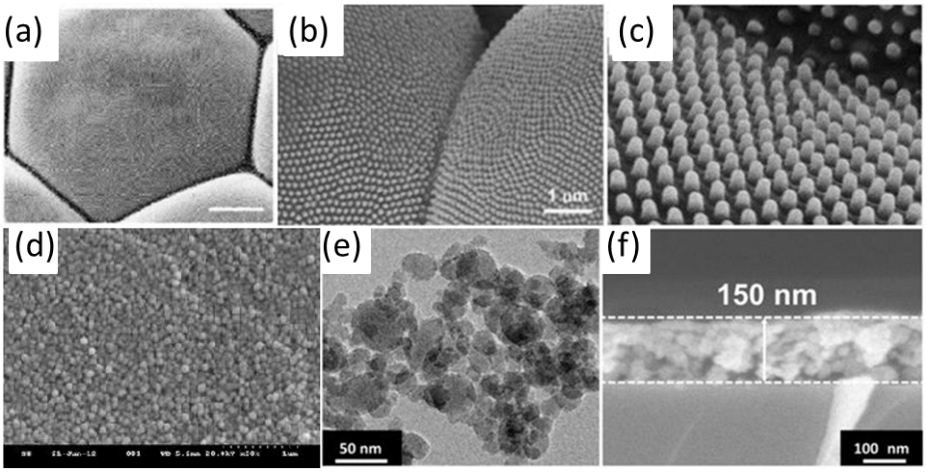

Figure 11. (a) The nipple array in one facet lens. (b) SEM image of two neighboring ommatidia. (c) Corneal nipple arrays. (d) Spray deposited particle-like TiO_2. (e) TEM image of the electrospun and subsequently sintered SiO_2 that forms the ARC. (f) Cross sectional SEM of the sub-wavelength thick SiO_2 ARC on glass.

(a) Reprinted with permission from[164]. Copyright2008 WILEY-VCH Verlag GmbH & Co. KGaA, Weinheim. (b) Reprinted with permission from[92]. Copyright 2011 Elsevier. (c) Reprinted with permission from[156]. Copyright 2010 Elsevier. (d) Reprinted with permission from[161]. Copyright 2013 Elsevier. (e-f) Reprinted with permission from[163]. Copyright 2013 Elsevier.

4.5. Spider silk

Spider dragline silk from the spider's orb-web is one of the most attractive materials available to date. The fiber is stronger than steel and has a tensile strength approaching that of Kevlar[165]. The feature of the hierarchical architecture of a spider silk are arranged with highly organized, densely H-bonded β-sheet nanocrystals within a semiamorphous protein matrix which consists of 3_1-helices and β-turn protein structures[166] (Fig.12). The perfect

mechanical performance of spider silk can be explained solely by structural effects[167]. The exceptional mechanical properties of spider silks arises from β-sheet nanocrystals that universally consist of highly conserved poly-(Gly-Ala) and poly-Ala repeats[168], by providing stiff orderly crosslinking domains embedded in a semi-amorphous matrix that consists predominantly of less orderly β-structures, helices and β-turns. β-Sheet nanocrystals also provide cohesion between the long polypeptide strands, enabling the amorphous domains to stretch significantly. When silk fibers are exposed to stretch, β-sheet nanocrystals reinforce the partially extended and oriented macromolecular chains by forming interlocking regions that transfer the load between chains under lateral loading[169,170].

A valid strategy for fabricating the spider silk-like fiber is to make use of materials similar to or same as the spider silk. Comparison of silkworm and spider silk reveals that both materials have a similar morphology[171], therefore scientists are inspired to take advantage of silkworm silk to simulate the spider dragline silk. Wang et al.[172] produced submicron diameter fibers with a coaxial internal structure with silkworm silk as core and a poly (ethylene oxide) (PEO) as shell using a two-fluid electrospinning technique. Then the silk/PEO fibers were annealed under high humidity to induce the conformation transformation from the random coil and/or silk I to predominantly β-sheet (silk II) structure. Finally, the PEO shell was extracted with water from the now insoluble silk core filament, resulting in a solid, crystallized silk fiber with diameter as small as 170 nm. Apart from silkworm silk, a novel silk-like protein, aneroin, which originates from the sea anemone N. Vectensis, has a highly similar sequence of decapeptide repeats in aneroin to that of spider silks[173]. Yang et al.[174] demonstrated for the first time the generation of this protein silk fibers by electrospinning. The methanol-treated as-spun fibers using aneroin with molecular weight of ~62kDa exhibited a better mechanical properties especially strength (~60 MPa) and stiffness (~1.8 GPa) which is similar to those of recombinant spider silks.

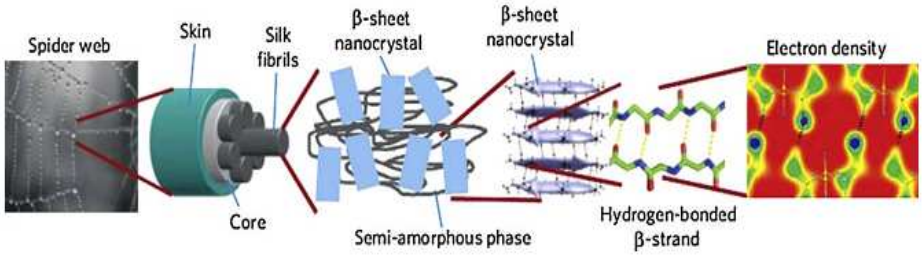

Figure 12. Schematic of the multiscale spider silk structure that ranges from nano to macro. It displays key structural features of silk, including the electron density at the Angstrom scale, hydrogen bonded β-strands, β-sheet nanocrystals, a hetero-nanocomposite of stiff nanocrystals embedded in a softer semi-amorphous phase and silk fibrils, which assembles into macroscopic silk fibers. Reprinted with permission from[169]. Copyright 2010 Nature Publishing Group.

4.6. Gecko's foot

Since 1872 the first documented study was reported of the mechanism by which geckos can walk on walls and ceilings [175], researchers have already studied the mechanism of gecko's adhesiveness[176-179]. Geckos are exceptional in their ability to climb rapidly up smooth vertical surfaces since they developed the most complex hierarchical surface structures capable of smart adhesion (Fig.13a). A gecko's foot possesses nearly five hundred thousand keratinous hairs or setae, namely approximately 14000 setae per mm^2 [180]and can produce 10 N of adhesive force with approximately 100 mm^2 of pad area[181] (Fig.13b). Each 30~130 μm long seta is only one-tenth the diameter of a human hair and contains hundreds to thousands of projections terminating in 0.2~0.5 μm spatula-shaped structures[182] (Fig.13c). One can predict that each seta should produce an average force of 20 μN and an average stress of 0.1 N

mm² (~1 atm) [177]. Van der Waals (vdW) forces are the primary mechanism utilized to adhere to surfaces[183,184], and capillary forces (as high as 100 KPa) created by humidity naturally present in the air are a secondary effect that can further increase adhesion force[176]. The attachment mechanism of van der Waals forces also apply to these examples: beetle[185], ladybug[184] and tree frog (Scynax perereca) [186] which all have the same or familiar hierarchical surface structures as the gecko's toe pad (Fig.13c). However, it is also found that electromagnetic (EM) radiation produced by the photoelectric effect allows the gecko to walk on walls and ceilings by electrostatic attraction[178].

In order to mimic the gecko's pad, an electrospun well-aligned nanofiber array is needed. Najem[187] collected nylon 6 electrospun fiber array using the rotating disc collector (RDC) (Fig.13d). By peeling it off the surface of the RDC and then placing it on a glass slide, he created gecko-inspired dry adhesives (Fig.13h). The dry adhesives are electrically insulating, and show strong shear adhesion strength of 27 N/cm^2. This measured value is 270% that reported of gecko feet and 97-fold above normal adhesion strength of the same arrays. Ballarin et al.[188] followed the idea of Najem[187] but collected Polycaprolactone (PCL) electrospun self-aligned fiber array with a tip collector (Fig.13e, f and g).The produced nanofiber array was then tested by a T-peel test, resulting adhesion strength of (758.7±211.7) KPa. The single contact adhesion energy value also suggested that vdW forces provided the primary adhesion mechanism. This study demonstrated how a principle saw in natural dry adhesive structures such as gecko toes which could be applied to a variety of synthetic electrospun materials. Their finding enables us to create electrically insulating dry adhesives with a strong shear adhesion and relatively weak normal adhesion for easy detachment.

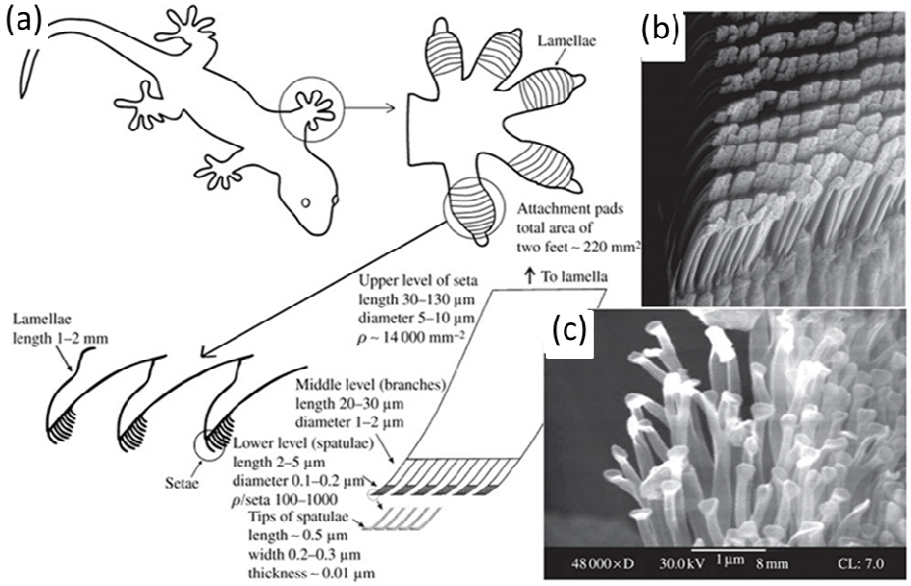

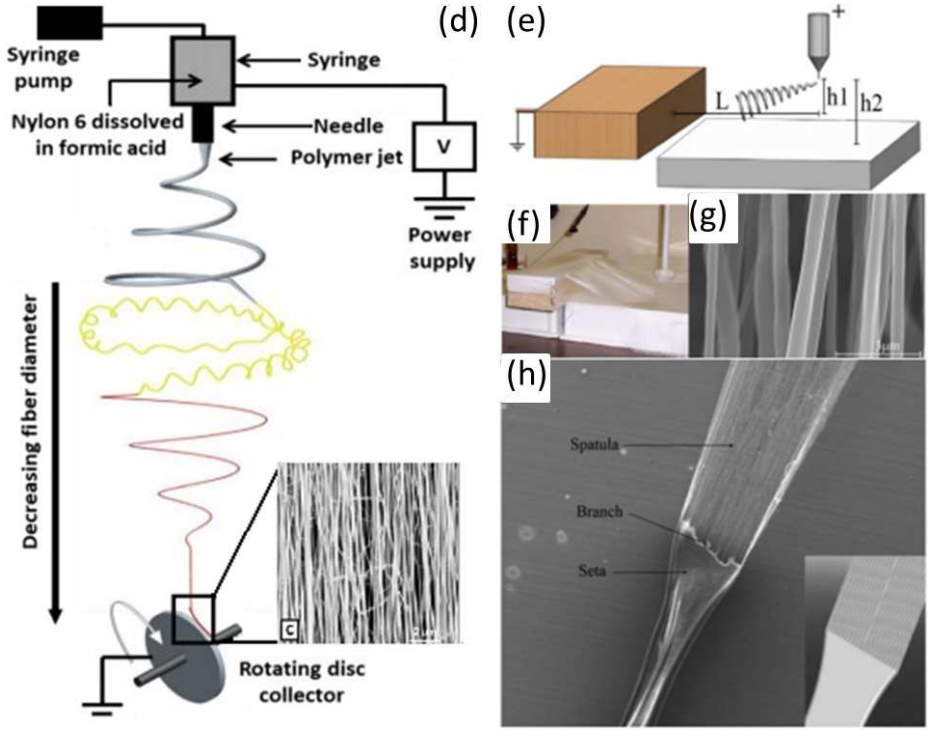

Figure 13. (a) Schematic drawings of a Tokay gecko including the overall body, one foot, a cross-sectional view of the lamellae, and an individual seta. ρ represents number of spatula. (b) Standard electron microscopy (SEM) image showing rows of setae on the bottom of a gecko's foot. (c) SEM image of spatulae on a gecko's foot. (d) Schematic of the electrospinning setup. (e) Tip collector electrospinning setup. (f) Macroscopic image of well aligned fibrous PCL membrane collected on the tip collector setup. (g) SEM micrograph of the well aligned fiber. (h) SEM micrograph of hierarchical structure, Insert: schematic diagram. (a) Reprinted with permission from[176]. Copyright 2007 Taylor & Francis. (b-c) Reprinted with permission from[189]. Copyright 2011 Royal Society of Chemistry. (d) Reprinted with permission from[187]. Copyright 2012 Corresponding author, University of Akron. (e-h) Reprinted with permission from[188]. Copyright 2013 Society of Plastics Engineers.

5. Design of animal-based hard tissue bio-materials

5.1. Bone

Bone refers to a family of materials that all have the mineralized collagen fibril as their basic building block[190]. The general structure of bone is a three-dimensional composite structure consisting of inorganic apatite crystals and organic collagen fibers[191] (Fig.14). Plate-shaped crystals, with 50×25 nm of length and width and with 2~3 nm thickness, of carbonated hydroxyapatite, with crystals aligned along their C-axis, are embedded in a type I collagen (Col) framework. The fibrils consist of triple-helix collagen chains with 1.5 nm diameter and 300 nm length and it's arranged in parallel arrays, with crystals aligned (sub-layers) [192]. Consecutive sublayers rotate through the lamellar plane by an average of 30º, forming a so-called plywood like structure. As each lamella is composed of five sub-layers, the total rotation is 150º, thus forming an asymmetric structure. Moreover, the collagen fibril bundles rotate around their axis within the five sub-layers[193]. Both facts enhance the isotropic properties of bone found at the macroscopic scale, as previously reported. Moreover, this type of architecture hinders crack propagation and increases toughness.

An attractive strategy for fabricating these types of composite biomaterials is to mimic the key features of nature bone. Ashrafet et al.[194] prepared polyvinyl alcohol (PVA)/Col/hydroxyapatite nanoparticles (nano-HAp)

composite nanofibers by electrospinning. It is of interest to observe that large numbers of HAp nanorods are preferentially oriented parallel to the longitudinal direction of the electrospun PVA/Col nanofibers. FTIR and thermal analysis demonstrated that there was strong intermolecular hydrogen bonding between the molecules of PVA/Col/n-Hap. Xie et al.[195] fabricated of "aligned-to-random" electrospun poly (lactic-co-glycolic acid) (PLGA) nanofiber scaffolds that mimic the structural organization of collagen fibers, where the aligned portion could mimic the high level of alignment for collagen fibers in a normal tendon that is responsible for a high tensile modulus and strength in the direction of muscle force and the random portion could recapitulate the less ordered organization of collagen fibers in a bone. Tests showed toughness of the aligned and random scaffolds were 142.5±97.9MPa and 52.7±24.2MPa, respectively.

When facing mimicking biomaterials with controlled structure, mechanical properties, and function, things seem to change to be difficult. However, there still exists experience scientists can draw the lessons of. Li et al.[191] prepared silk/apatite composites (an amorphous of β-sheet) by growing apatite on functionalized nanodiameter silk fibroin fibers by electrospinning. The functionalized fibers were spun from an aqueous solution of silk/PEO containing poly (L-aspartate) (poly-Asp), which was introduced as an analogue of noncollageous proteins normally found in bone. Silk fibroin associated with the acidic poly-Asp and acted as template for mineralization. Apatite mineral growth occurred preferentially along the longitudinal direction of the fibers. The results suggest that this approach can be used to form structures with potential utility for bone-related biomaterials based on the ability to control the interface wherein nucleation and crystal growth occur on the silk fibroin.

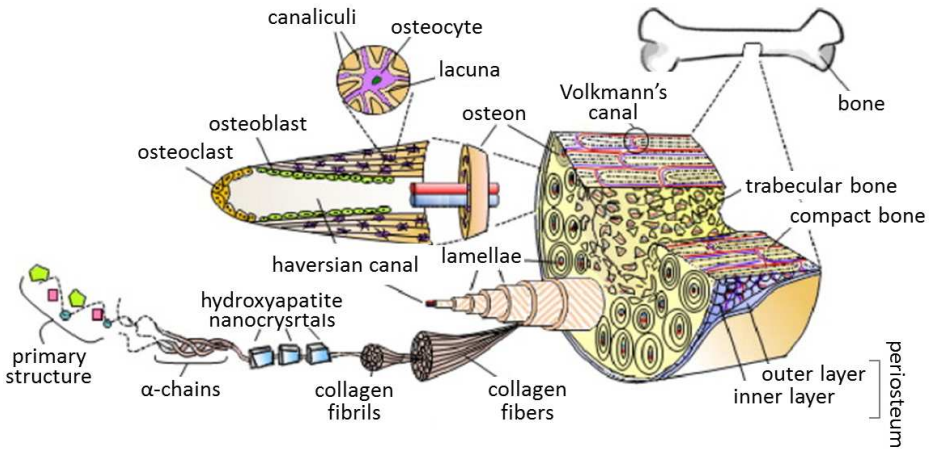

Figure 14. The hierarchical organization of bone. Plate-shaped crystals, of carbonated hydroxyapatite, with crystals aligned along their c-axis, are embedded in a type-I collagen framework. The fibrils consist of triple-helix collagen chains with 1.5 nm diameter and 300 nm length. The apatite crystals are nucleated at specific regions on or within the collagen fibrils. Reprinted with permission from [192]. Copyright 2010 Elsevier.

6. Conclusions and outlook

It is clear that nature has a large number of materials and structures with rather unique characteristics and the emerging field of biomimetic is already gaining an increasing attention in the scientific and technical arena. Electrospinning has succeeded within the last years in establishing itself as an internationally highly recognized enabeling method granting access to a broad range of functional structures. This review provides an overview of typical structures of the organisms and recent developments in controlled fabrications of well-defined bio-inspired structures of nanomaterials via electrospinning. As we understand what these properties originated from, we can

begin to exploit them for commercial applications, like solar cell, sunlight splitting catalysts, biomedical implants and self-cleaning fabric.

Although great achievements have been accomplished in this field through years of efforts, current work is not going as we expect as there are still many challenges. An important issue that should be mentioned is accurately analyzing about the structures of biomimetic materials. For example, it is found that wax exists on the surface of many plants and animals[196,197] (e.g., the lotus leaf, rice leaf and water strider leg) and whether the wax on the surface has a significant impact on the property (e.g., superhydrophobicity) should be analyzed. Another issue that hampered researchers move forward is that current research work are almost focus on the one functional property. How to design composite functional or function integrated materials is still facing the challenges. For example, lotus leaves are famous for their superhydrophobic, low adhesive and self-cleaning properties due to the micro-papillae structure. Butterfly wings present superhydrophobicity, directional adhesion, structural color, self-cleaning, chemical sensing capability, and fluorescence emission functions depending on the multiscale structures[198]. As a result, studying the structure-property correlation especially when electrospinning is combined with at least one biomimetic or bio-inspired method or even an array of methods is of significant importance. In addition, it is important to match the material's structure and property to the desired practical condition which of course is sometimes a complicated process. One may want to systematically design "biomimetic materials", the objective of which is to seek deeper insights into mechanisms being up to the structures as well as achieving higher performance.

Opportunity is always accompanied with challenges, thus electrospinning can be expected to contribute greatly to further advances in nanotechnology and future researches, which will proceed in the area of controlled arrangements of electrospun nanofibers and their potential applications.

References:

1. Bar-Cohen Y. Biomimetics: biologically inspired technologies: CRC Press; 2005.

2. Schmitt OH. Some interesting and useful biomimetic transforms. Proceeding, Third International Biophysics Congress. Boston, 1969:297.

3. Harkness JM. In Appreciation?A Lifetime of Connections: Otto Herbert Schmitt, 1913 - 1998. Physics in Perspective. 2002 2002-12-01;4(4):456-90.

4. Vincent JF, Bogatyreva OA, Bogatyrev NR, Bowyer A, Pahl A. Biomimetics: its practice and theory. Journal of the Royal Society Interface. 2006;3(9):471-82.

5. Guo Z, Zhou F, Hao J, Liu W. Effects of system parameters on making aluminum alloy lotus. J Colloid Interf Sci. 2006;303(1):298-305.

6. Yu Q, Zeng Z, Zhao W, Li M, Wu X, Xue Q. Fabrication of adhesive superhydrophobic Ni-Cu-P alloy coatings with high mechanical strength by one step electrodeposition. Colloids and Surfaces A: Physicochemical and Engineering Aspects. 2013;427(20):1-6.

7. Chen Z, Hao L, Duan M, Chen C. Electrodeposition fabrication of Co-based superhydrophobic powder coatings in non-aqueous electrolyte. Applied Physics A. 2013;111(2):581-5.

8. Schubert B, Majidi C, Groff RE, et al. Towards friction and adhesion from high modulus microfiber arrays. J Adhes Sci Technol. 2007;21(12-13):1297-315.

9. Büttner CC, Schulz U. Shark Skin Inspired Riblet Coatings for Aerodynamically Optimized High Temperature Applications in Aeroengines. Adv Eng Mater. 2011 2011-04-01;13(4):288-95.

10. Li Y, Li L, Sun J. Bioinspired Self-Healing Superhydrophobic Coatings. Angewandte Chemie International Edition.

2010 2010-08-16;49(35):6129-33.

11. Watanabe K, Hoshino T, Kanda K, Haruyama Y, Kaito T, Matsui S. Optical measurement and fabrication from a Morpho-butterfly-scale quasistructure by focused ion beam chemical vapor deposition. Journal of Vacuum Science \& Technology B: Microelectronics and Nanometer Structures. 2005;23(2):570-4.

12. Li D, Zhao AW, Wang DP, et al. Effect of Top Structure on Adhesion of Carbon Nanotubes Based Gecko Inspired Dry Adhesive. Applied Mechanics and Materials. 2014;461:381-7.

13. DeNatale JF, Hood PJ, Flintoff JF, Harker AB. Fabrication and characterization of diamond moth eye antireflective surfaces on Ge. Journal of Applied Physics. 1992;71(3):1388-93.

14. F U Rstner R, Barthlott W, Neinhuis C, Walzel P. Wetting and self-cleaning properties of artificial superhydrophobic surfaces. Langmuir. 2005;21(3):956-61.

15. Kang S, Tai T, Fang T. Replication of butterfly wing microstructures using molding lithography. Current Applied Physics. 2010;10(2):625-30.

16. C BC, U S. Shark skin inspired riblet structures as aerodynamically optimized high temperature coatings for blades of aeroengines. Smart Materials and Structures. 2011;20(9):94016.

17. Li Y, Zhang J, Zhu S, et al. Bioinspired Silica Surfaces with Near-Infrared Improved Transmittance and Superhydrophobicity by Colloidal Lithography. Langmuir. 2010 2010-03-04;26(12):9842-7.

18. Silver J, Withnall R, Ireland TG, Fern GR. Novel nano-structured phosphor materials cast from natural Morpho butterfly scales. J Mod Optic. 2005;52(7):999-1007.

19. Sun M, Luo C, Xu L, et al. Artificial lotus leaf by nanocasting. Langmuir. 2005;21(19):8978-81.

20. Kustandi TS, Samper VD, Ng WS, Chong AS, Gao H. Fabrication of a gecko-like hierarchical fibril array using a bonded porous alumina template. J Micromech Microeng. 2007;17(10):N75.

21. Xi J, Jiang L. Biomimic superhydrophobic surface with high adhesive forces. Industrial & Engineering Chemistry Research. 2008;47(17):6354-7.

22. Zhao W, Wang L, Xue Q. Fabrication of low and high adhesion hydrophobic Au surfaces with micro/nano-biomimetic structures. The Journal of Physical Chemistry C. 2010;114(26):11509-14.

23. Min W, Jiang B, Jiang P. Bioinspired Self-Cleaning Antireflection Coatings. Adv Mater. 2008 2008-10-17;20(20):3914-8.

24. Baldacchini T, Carey JE, Zhou M, Mazur E. Superhydrophobic Surfaces Prepared by Microstructuring of Silicon Using a Femtosecond Laser. Langmuir. 2006 2006-04-19;22(11):4917-9.

25. Cortese B, D'Amone S, Manca M, Viola I, Cingolani R, Gigli G. Superhydrophobicity Due to the Hierarchical Scale Roughness of PDMS Surfaces. Langmuir. 2008 2008-01-25;24(6):2712-8.

26. Wohlfart E, Fern A Ndez-Bl A Zquez JP, Knoche E, et al. Nanofibrillar patterns by plasma etching: The influence of polymer crystallinity and orientation in surface morphology. Macromolecules. 2010;43(23):9908-17.

27. Vernon JP, Fang Y, Cai Y, Sandhage KH. Morphology-Preserving Conversion of a 3D Bioorganic Template into a Nanocrystalline Multicomponent Oxide Compound. Angewandte Chemie. 2010 2010-10-11;122(42):7931-4.

28. Podsiadlo P, Paternel S, Rouillard J, et al. Layer-by-layer assembly of nacre-like nanostructured composites with antimicrobial properties. Langmuir. 2005;21(25):11915-21.

29. Shi F, Wang Z, Zhang X. Combining a Layer-by-Layer Assembling Technique with Electrochemical Deposition of Gold Aggregates to Mimic the Legs of Water Striders. Adv Mater. 2005;17(8):1005-9.

30. Zhao Y, Li M, Lu Q, Shi Z. Superhydrophobic Polyimide Films with a Hierarchical Topography: Combined Replica Molding and Layer-by-Layer Assembly. Langmuir. 2008 2008-10-10;24(21):12651-7.

31. Chang T, Chen S, Chan C, Chen C, Lee C. Fabrication of 3-dimension photonic crystal using self assembly and autocloning technologies., 2007.

32. Yao H, Tan Z, Fang H, Yu S. Artificial Nacre-like Bionanocomposite Films from the Self-Assembly of Chitosan–Montmorillonite Hybrid Building Blocks. Angewandte Chemie International Edition. 2010 2010-12-27;49(52):10127-31.

33. Chunder A, Etcheverry K, Wadsworth S, Boreman GD, Zhai L. Fabrication of anti-reflection coatings on plastics

using the spraying layer-by-layer self-assembly technique. Journal of the Society for Information Display. 2009 2009-04-01;17(4):389-95.

34. Peng Y, Lo K, Juang Y. Constructing a Superhydrophobic Surface on Polydimethylsiloxane via Spin Coating and Vapor−Liquid Sol−Gel Process. Langmuir. 2009 2009-12-18;26(7):5167-71.

35. Weatherspoon MR, Cai Y, Crne M, Srinivasarao M, Sandhage KH. 3D Rutile Titania-Based Structures with Morpho Butterfly Wing Scale Morphologies. Angewandte Chemie International Edition. 2008 2008-09-29;47(41):7921-3.

36. Tadanaga K, Yamaguchi N, Uraoka Y, Matsuda A, Minami T, Tatsumisago M. Anti-reflective properties of nano-structured alumina thin films on poly(methyl methacrylate) substrates by the sol–gel process with hot water treatment. Thin Solid Films. 2008;516(14):4526-9.

37. Feng L, Liu Y, Zhang H, Wang Y, Qiang X. Superhydrophobic alumina surface with high adhesive force and long-term stability. Colloids and Surfaces A: Physicochemical and Engineering Aspects. 2012;410:66-71.

38. Kokubo T. Design of bioactive bone substitutes based on biomineralization process. Materials Science and Engineering: C. 2005;25(2):97-104.

39. Fu G, Valiyaveettil S, Wopenka B, Morse DE. CaCO3 biomineralization: acidic 8-kDa proteins isolated from aragonitic abalone shell nacre can specifically modify calcite crystal morphology. 2005;6(3):1289-98.

40. Addadi L, Joester D, Nudelman F, Weiner S. Mollusk Shell Formation: A Source of New Concepts for Understanding Biomineralization Processes. Chemistry – A European Journal. 2006 2006-01-23;12(4):980-7.

41. Sone ED, Weiner S, Addadi L. Biomineralization of limpet teeth: A cryo-TEM study of the organic matrix and the onset of mineral deposition. J Struct Biol. 2007;158(3):428-44.

42. Lazaris A, Arcidiacono S, Huang Y, et al. Spider silk fibers spun from soluble recombinant silk produced in mammalian cells. Science. 2002;295(5554):472-6.

43. Xia X, Qian Z, Ki CS, Park YH, Kaplan DL, Lee SY. Native-sized recombinant spider silk protein produced in metabolically engineered Escherichia coli results in a strong fiber. Proceedings of the National Academy of Sciences. 2010;107(32):14059-63.

44. Teulé F, Cooper AR, Furin WA, et al. A protocol for the production of recombinant spider silk-like proteins for artificial fiber spinning. Nature Protocols. 2009;4(3):341-55.

45. Heng L, Wang X, Dong Y, et al. Bio-Inspired Fabrication of Lotus Leaf Like Membranes as Fluorescent Sensing Materials. Chemistry-An Asian Journal. 2008;3(6):1041-5.

46. Ma M, Hill RM, Rutledge GC. A review of recent results on superhydrophobic materials based on micro-and nanofibers. J Adhes Sci Technol. 2008;22(15):1799-817.

47. Rayleigh L. On the equilibrium of liquid conducting masses charged with electricity. The London, Edinburgh, and Dublin Philosophical Magazine and Journal of Science. 1882;14(87):184-6.

48. Zeleny J. The electrical discharge from liquid points, and a hydrostatic method of measuring the electric intensity at their surfaces. Physical Review. 1914;3(2):69.

49. Formhals A; Process and apparatus for preparing artificial threads. 1934 1930-12-05.

50. Taylor G. Disintegration of water drops in an electric field. Proceedings of the Royal Society of London. Series A. Mathematical and Physical Sciences. 1964;280(1382):383-97.

51. Taylor GI, McEwan AD. The stability of a horizontal fluid interface in a vertical electric field. J. Fluid Mech. 1965;22(1):1-15.

52. Taylor G. Electrically driven jets. Proceedings of the Royal Society of London. A. Mathematical and Physical Sciences. 1969;313(1515):453-75.

53. Sun B, Long Y, Chen Z, et al. Recent advances in flexible and stretchable electronic devices via electrospinning. Journal of Materials Chemistry C. 2014;2(7):1209-19.

54. Li D, Xia Y. Electrospinning of Nanofibers: Reinventing the Wheel? Adv Mater. 2004 2004-07-19;16(14):1151-70.

55. Reneker DH, Yarin AL. Electrospinning jets and polymer nanofibers. Polymer. 2008 2008-05-13;49(10):2387-425.

56. Sun B, Long YZ, Zhang HD, et al. Advances in three-dimensional nanofibrous macrostructures via electrospinning.

Prog Polym Sci. 2014;39(5):862-90.

57. Bhardwaj N, Kundu SC. Electrospinning: a fascinating fiber fabrication technique. Biotechnol Adv. 2010;28(3):325-47.

58. Nuraje N, Khan WS, Lei Y, Ceylan M, Asmatulu R. Superhydrophobic electrospun nanofibers. Journal of Materials Chemistry A. 2013;1:1929-46.

59. Teo W, Inai R, Ramakrishna S. Technological advances in electrospinning of nanofibers. Science and Technology of Advanced Materials. 2011;12(1):13002.

60. Subbiah T, Bhat GS, Tock RW, Parameswaran S, Ramkumar SS. Electrospinning of nanofibers. J Appl Polym Sci. 2005;96(2):557-69.

61. Teo WE, Ramakrishna S. A review on electrospinning design and nanofibre assemblies. Nanotechnology. 2006;17(14):R89.

62. He J, Liu Y, Xu L. Apparatus for preparing electrospun nanofibres: a comparative review. Mater Sci Tech-Lond. 2010;26(11):1275-87.

63. Niu H, Wang X, Lin T. Needleless electrospinning: developments and performances. Nanofibers-Production, Properties and Functional Applications. InTech. 2011.

64. Nayak R, Padhye R, Kyratzis IL, Truong YB, Arnold L. Recent advances in nanofibre fabrication techniques. Text Res J. 2012;82(2):129-47.

65. Niu H, Wang X, Lin T. Upward needleless electrospinning of nanofibers. Journal of engineered fibers and fabrics. 2012;7(3):17-22.

66. Zander NE. Hierarchically Structured Electrospun Fibers. Polymers. 2013;5(1):19-44.

67. Wang X, Ding B, Sun G, Wang M, Yu J. Electro-spinning/netting: A strategy for the fabrication of three-dimensional polymer nano-fiber/nets. Prog Mater Sci. 2013 2013-10-01;58(8):1173-243.

68. Teo W, Ramakrishna S. Electrospun nanofibers as a platform for multifunctional, hierarchically organized nanocomposite. Compos Sci Technol. 2009;69(11):1804-17.

69. Huang Z, Zhang YZ, Kotaki M, Ramakrishna S. A review on polymer nanofibers by electrospinning and their applications in nanocomposites. Compos Sci Technol. 2003 2014-02-24;63(15):2223-53.

70. Ding B, Wang M, Wang X, Yu J, Sun G. Electrospun nanomaterials for ultrasensitive sensors. Materials Today. 2010 2010-11-01;13(11):16-27.

71. Koombhongse S, Liu W, Reneker DH. Flat polymer ribbons and other shapes by electrospinning. Journal of Polymer Science Part B: Polymer Physics. 2001 2001-11-01;39(21):2598-606.

72. Barthlott W, Neinhuis C. Purity of the sacred lotus, or escape from contamination in biological surfaces. Planta. 1997;202(1):1-8.

73. Cheng YT, Rodak DE, Wong CA, Hayden CA. Effects of micro-and nano-structures on the self-cleaning behaviour of lotus leaves. Nanotechnology. 2006;17(5):1359.

74. Patankar NA. Transition between superhydrophobic states on rough surfaces. Langmuir. 2004;20(17):7097-102.

75. Cheng Y, Rodak DE. Is the lotus leaf superhydrophobic? Appl Phys Lett. 2005 2005-01-01;86(14):144101.

76. Marmur A. The lotus effect: superhydrophobicity and metastability. Langmuir. 2004;20(9):3517-9.

77. Jiang L, Zhao Y, Zhai J. A Lotus-Leaf-like Superhydrophobic Surface: A Porous Microsphere/Nanofiber Composite Film Prepared by Electrohydrodynamics. Angewandte Chemie. 2004;116(33):4438-41.

78. Qu M, Zhao G, Cao X, Zhang J. Biomimetic fabrication of lotus-leaf-like structured polyaniline film with stable superhydrophobic and conductive properties. Langmuir. 2008;24(8):4185-9.

79. Dai S, Ding W, Wang Y, Zhang D, Du Z. Fabrication of hydrophobic inorganic coatings on natural lotus leaves for nanoimprint stamps. Thin Solid Films. 2011 2011-06-01;519(16):5523-7.

80. McLauchlin ML, Yang D, Aella P, Garcia AA, Picraux ST, Hayes MA. Evaporative properties and pinning strength of laser-ablated, hydrophilic sites on lotus-leaf-like, nanostructured surfaces. Langmuir. 2007;23(9):4871-7.

81. Huang Z, Zhu Y, Zhang J, Yin G. Stable biomimetic superhydrophobicity and magnetization film with Cu-ferrite

nanorods. The Journal of Physical Chemistry C. 2007;111(18):6821-5.
82. Liu K, Yao X, Jiang L. Recent developments in bio-inspired special wettability. Chem Soc Rev. 2010;39(8):3240-55.
83. Sun T, Feng L, Gao X, Jiang L. Bioinspired Surfaces with Special Wettability. Accounts Chem Res. 2005 2005-05-19;38(8):644-52.
84. Patankar NA. Mimicking the lotus effect: influence of double roughness structures and slender pillars. Langmuir. 2004;20(19):8209-13.
85. Guo Z, Liu W. Biomimic from the superhydrophobic plant leaves in nature: Binary structure and unitary structure. Plant Sci. 2007;172(6):1103-12.
86. Feng XJ, Jiang L. Design and creation of superwetting/antiwetting surfaces. Adv Mater. 2006;18(23):3063-78.
87. Yoon H, Park JH, Kim GH. A Superhydrophobic Surface Fabricated by an Electrostatic Process. Macromol Rapid Comm. 2010 2010-08-17;31(16):1435-9.
88. Lee MS, Lee TS, Park WH. Highly hydrophobic nanofibrous surfaces genearated by poly (vinylidene fluoride). Fibers and Polymers. 2013;14(8):1271-5.
89. Soeno T, Inokuchi K, Shiratori S. Ultra Water-Repellent Surface Resulting from Complicated Microstructure of SiO2 nano particles. TRANSACTIONS-MATERIALS RESEARCH SOCIETY OF JAPAN. 2003;28(4):1207.
90. Ma M, Gupta M, Li Z, et al. Decorated electrospun fibers exhibiting superhydrophobicity. Adv Mater. 2007;19(2):255-9.
91. Miyauchi Y, Ding B, Shiratori S. Fabrication of a silver-ragwort-leaf-like super-hydrophobic micro/nanoporous fibrous mat surface by electrospinning. Nanotechnology. 2006;17(20):5151.
92. Gu Z, Wei H, Zhang R, et al. Artificial silver ragwort surface. Appl Phys Lett. 2005;86(20):201915.
93. Priya ARS, Subramania A, Jung Y, Kim K. High-Performance Quasi-Solid-State Dye-Sensitized Solar Cell Based on an Electrospun PVdF−HFP Membrane Electrolyte. Langmuir. 2008 2008-08-02;24(17):9816-9.
94. Ahmed F, Choudhury NR, Dutta NK, Zannettino A, Knott R. Near superhydrophobic fibrous scaffold for endothelialization: fabrication, characterization and cellular activities. Biomacromolecules. 2013 2013-11-11;14(11):3850-60.
95. Lee TD, Dong Q, Lee BH, et al. Study of Superhydrophobic by Electrospun PVdF-HFP Fibers with Plasma Treatment. 9th International Conference on Fracture & Strength of Solids. Jeju, Korea, 2013.
96. Zheng J, He A, Li J, Xu J, Han CC. Studies on the controlled morphology and wettability of polystyrene surfaces by electrospinning or electrospraying. Polymer. 2006 2006-09-20;47(20):7095-102.
97. Kang M, Jung R, Kim H, Jin H. Preparation of superhydrophobic polystyrene membranes by electrospinning. Colloids and Surfaces A: Physicochemical and Engineering Aspects. 2008 2008-02-01;313 – 314:411-4.
98. Lin J, Cai Y, Wang X, Ding B, Yu J, Wang M. Fabrication of biomimetic superhydrophobic surfaces inspired by lotus leaf and silver ragwort leaf. Nanoscale. 2011;3(3):1258-62.
99. Lin J, Wang X, Ding B, Yu J, Sun G, Wang M. Biomimicry via electrospinning. Crit Rev Solid State. 2012;37(2):94-114.
100. Ge L, Wang X, Tu Z, et al. Fabrication of Multilayered Hollow Nanofibers and Estimation of Its Young's Modulus. JAPANESE JOURNAL OF APPLIED PHYSICS PART 1 REGULAR PAPERS SHORT NOTES AND REVIEW PAPERS. 2007;46(10A):6790.
101. Chen Y, He B, Lee J, Patankar NA. Anisotropy in the wetting of rough surfaces. J Colloid Interf Sci. 2005;281(2):458-64.
102. Gao X, Yao X, Jiang L. Effects of rugged nanoprotrusions on the surface hydrophobicity and water adhesion of anisotropic micropatterns. Langmuir. 2007;23(9):4886-91.
103. Choi W, Tuteja A, Mabry JM, Cohen RE, McKinley GH. A modified Cassie – Baxter relationship to explain contact angle hysteresis and anisotropy on non-wetting textured surfaces. J Colloid Interf Sci. 2009 2009-11-01;339(1):208-16.
104. Gao J, Liu Y, Xu H, Wang Z, Zhang X. Mimicking biological structured surfaces by phase-separation micromolding. Langmuir. 2009;25(8):4365-9.

105. Zhang F, Low HY. Anisotropic wettability on imprinted hierarchical structures. Langmuir. 2007;23(14):7793-8.
106. Wu D, Wang J, Wu S, et al. Three-Level Biomimetic Rice-Leaf Surfaces with Controllable Anisotropic Sliding. Adv Funct Mater. 2011;21(15):2927-32.
107. Lee SG, Lim HS, Lee DY, Kwak D, Cho K. Tunable Anisotropic Wettability of Rice Leaf-Like Wavy Surfaces. Adv Funct Mater. 2012.
108. Yao J, Wang J, Yu Y, Yang H, Xu Y. Biomimetic fabrication and characterization of an artificial rice leaf surface with anisotropic wetting. Chinese Science Bulletin. 2012;57(20):2631-4.
109. Zhan N, Li Y, Zhang C, et al. A novel multinozzle electrospinning process for preparing superhydrophobic PS films with controllable bead-on-string/microfiber morphology. J Colloid Interf Sci. 2010 2010-05-15;345(2):491-5.
110. Ma M, Mao Y, Gupta M, Gleason KK, Rutledge GC. Superhydrophobic fabrics produced by electrospinning and chemical vapor deposition. Macromolecules. 2005;38(23):9742-8.
111. Feng X, Gao X, Wu Z, Jiang L, Zheng Q. Superior water repellency of water strider legs with hierarchical structures: experiments and analysis. Langmuir. 2007;23(9):4892-6.
112. Hu DL, Chan B, Bush JW. The hydrodynamics of water strider locomotion. Nature. 2003;424(6949):663-6.
113. Shi F, Niu J, Liu J, et al. Towards understanding why a superhydrophobic coating is needed by water striders. Adv Mater. 2007;19(17):2257-61.
114. Zheng Q, Yu Y, Feng X. The role of adaptive-deformation of water strider leg in its walking on water. J Adhes Sci Technol. 2009;23(3):493-501.
115. Watson GS, Cribb BW, Watson JA. Experimental determination of the efficiency of nanostructuring on non-wetting legs of the water strider. Acta Biomaterialia. 2010;6(10):4060-4.
116. Gao X, Jiang L. Biophysics: water-repellent legs of water striders. Nature. 2004;432(7013):36.
117. Bush JWM, Hu DL, Prakash M. The Integument of Water-walking Arthropods: Form and Function. Adv Insect Physiol. 2007;34:117-92.
118. Wu H, Zhang R, Sun Y, et al. Biomimetic nanofiber patterns with controlled wettability. Soft Matter. 2008;4(12):2429-33.
119. Xue Y, Wang H, Yu D, et al. Superhydrophobic electrospun POSS-PMMA copolymer fibres with highly ordered nanofibrillar and surface structures. Chem Commun. 2009(42):6418-20.
120. Feng X, Gao X, Wu Z, Jiang L, Zheng Q. Superior water repellency of water strider legs with hierarchical structures: experiments and analysis. Langmuir. 2007;23(9):4892-6.
121. Liu Y, Chen X, Xin JH. Hydrophobic duck feathers and their simulation on textile substrates for water repellent treatment. Bioinspiration & Biomimetics. 2008;3(4):46007.
122. Bormashenko E, Bormashenko Y, Stein T, Whyman G, Bormashenko E. Why do pigeon feathers repel water? Hydrophobicity of pennae, Cassie – Baxter wetting hypothesis and Cassie – Wenzel capillarity-induced wetting transition. J Colloid Interf Sci. 2007 2007-07-01;311(1):212-6.
123. Rijke AM, Jesser WA, Evans SW, Bouwman H. Water repellency and feather structure of the blue swallow Hirundo atrocaerulea. Ostrich. 2000;71(1-2):143-5.
124. Wu H, Fan J, Wan X, Du N. One-step fabrication of branched poly (vinyl alcohol) nanofibers by magnetic coaxial electrospinning. J Appl Polym Sci. 2012;125(2):1425-9.
125. Martina R, Sundarrajan S, Pliszka D, Ramakrishna S, Modesti M. Multifunctional membranes based on spinning technologies: the synergy of nanofibers and nanoparticles. Nanotechnology. 2008;19(28):28575.
126. Teo WE, Ramakrishna S. Electrospun fibre bundle made of aligned nanofibres over two fixed points. Nanotechnology. 2005;16(9):1878.
127. Lei F, Qu Y, Gan Y, Gebauer A, Kaiser M. The feather microstructure of Passerine sparrows in China. Journal fur Ornithologie. 2002;143(2):205-12.
128. Qiu P, Mao C. Biomimetic branched hollow fibers templated by self-assembled fibrous polyvinylpyrrolidone structures in aqueous solution. ACS nano. 2010;4(3):1573-9.

129. Li F, Zhao Y, Song Y. Core-Shell nanofibers: Nano channel and capsule by coaxial electrospinning. In: Kumar A (ed). Nanofibers: In Tech, 2010.
130. Yong Z, Xinyu C, Lei J. Bio-mimic Multichannel Microtubes by a Facile Method. J Am Chem Soc. 2007;129(4):764-5.
131. Meyers MA, Chen P, Lin AY, Seki Y. Biological materials: Structure and mechanical properties. Prog Mater Sci. 2008 2008-01-01;53(1):1-206.
132. Srinivasarao M, Others. Nano-optics in the biological world: beetles, butterflies, birds, and moths. Chemical Reviews-Columbus. 1999;99(7):1935-62.
133. Kinoshita S, Yoshioka S, Kawagoe K. Mechanisms of structural colour in the Morpho butterfly: cooperation of regularity and irregularity in an iridescent scale. Proceedings of the Royal Society of London. Series B: Biological Sciences. 2002;269(1499):1417-21.
134. Yoshioka S, Kinoshita S. Wavelength--selective and anisotropic light--diffusing scale on the wing of the Morpho butterfly. Proceedings of the Royal Society of London. Series B: Biological Sciences. 2004;271(1539):581-7.
135. Tabata H, Kumazawa K, Funakawa M, Takimoto J, Akimoto M. Microstructures and optical properties of scales of butterfly wings. Opt Rev. 1996;3(2):139-45.
136. Vukusic P, Sambles JR, Lawrence CR, Wootton RJ. Quantified interference and diffraction in single Morpho butterfly scales. Proceedings of the Royal Society of London. Series B: Biological Sciences. 1999;266(1427):1403-11.
137. Yoshioka S, Kinoshita S. Structural or pigmentary? Origin of the distinctive white stripe on the blue wing of a Morpho butterfly. Proceedings of the Royal Society B: Biological Sciences. 2006;273(1583):129-34.
138. Ding Y, Xu S, Wang ZL. Structural colors from Morpho peleides butterfly wing scales. J Appl Phys. 2009;106(7):74702.
139. Huang J, Wang X, Wang ZL. Controlled replication of butterfly wings for achieving tunable photonic properties. Nano Lett. 2006;6(10):2325-31.
140. Kang S, Tai T, Fang T. Replication of butterfly wing microstructures using molding lithography. Current Applied Physics. 2010 2010-03-01;10(2):625-30.
141. Weatherspoon MR, Cai Y, Crne M, Srinivasarao M, Sandhage KH. 3D Rutile Titania-Based Structures with Morpho Butterfly Wing Scale Morphologies. Angewandte Chemie International Edition. 2008;47(41):7921-3.
142. Kustandi TS, Low HY, Teng JH, Rodriguez I, Yin R. Mimicking Domino-Like Photonic Nanostructures on Butterfly Wings. Small. 2009;5(5):574-8.
143. Zhang Y, Chen Q, Jin Z, Kim E, Sun H. Biomimetic graphene films and their properties. Nanoscale. 2012;4(16):4858-69.
144. Vukusic P, Sambles JR. Shedding light on butterfly wings., 2001:85-95.
145. Lou S, Guo X, Fan T, Zhang D. Butterflies: inspiration for solar cells and sunlight water-splitting catalysts. Energy & Environmental Science. 2012;5(11):9195-216.
146. Chen Y, Chang Y, Huang J, Chen I, Kuo C. Light Scattering and Enhanced Photoactivities of Electrospun Titania Nanofibers. The Journal of Physical Chemistry C. 2012;116(5):3857-65.
147. Shang M, Wang W, Zhang L, Sun S, Wang L, Zhou L. 3D Bi2WO6/TiO2 Hierarchical Heterostructure: Controllable Synthesis and Enhanced Visible Photocatalytic Degradation Performances. The Journal of Physical Chemistry C. 2009 2013-04-01;113(33):14727-31.
148. Kuwayama H, Matsumoto H, Morota K, Minagawa M, Tanioka A. Control over color of nanotextured coatings by electrospray deposition. Sen'i Gakkaishi. 2008;64(1):1-4.
149. Ma M. Nanostructured electrospun fibers: from superhydrophobicity to block copolymer self-assembly [phdma2008nanostructured,]: Massachusetts Institute of Technology, 2008.
150. Bernhard CG. Structural and functional adaptation in a visual system. Endeavour. 1967;26:79-84.
151. Clapham PB, Hutley MC. Reduction of lens reflexion by the “Moth Eye” principle. Nature. 1973;244(5414):281-2.
152. Stavenga DG, Foletti S, Palasantzas G, Arikawa K. Light on the moth-eye corneal nipple array of butterflies.

Proceedings of the Royal Society B: Biological Sciences. 2006;273(1587):661-7.
153. Dewan R, Fischer S, Meyer-Rochow VB, O Zdemir Y, Hamraz S, Knipp D. Studying nanostructured nipple arrays of moth eye facets helps to design better thin film solar cells. Bioinspiration & biomimetics. 2012;7(1):16003.
154. Li Y, Zhang J, Yang B. Antireflective surfaces based on biomimetic nanopillared arrays. Nano Today. 2010;5(2):117-27.
155. Yamada N, Kim ON, Tokimitsu T, Nakai Y, Masuda H. Optimization of anti-reflection moth-eye structures for use in crystalline silicon solar cells. Progress in Photovoltaics: Research and Applications. 2011;19(2):134-40.
156. Sun C, Jiang P, Jiang B. Broadband moth-eye antireflection coatings on silicon. Appl Phys Lett. 2008;92(6):61112.
157. Striemer CC, Fauchet PM. Dynamic etching of silicon for broadband antireflection applications. Appl Phys Lett. 2002;81(16):2980-2.
158. Yao L, He J. Recent progress in antireflection and self-cleaning technology – From surface engineering to functional surfaces. Prog Mater Sci. 2014;61:94-143.
159. Li F, Li Q, Kim H. Spray deposition of electrospun TiO2 nanoparticles with self-cleaning and transparent properties onto glass. Applied Surface Science. 2013;276:390-6.
160. Raut HK, Ganesh VA, Nair AS, Ramakrishna S. Anti-reflective coatings: A critical, in-depth review. Energy & Environmental Science. 2011;4(10):3779-804.
161. Raut HK, Nair AS, Dinachali SS, Ganesh VA, Walsh TM, Ramakrishna S. Porous SiO2 anti-reflective coatings on large-area substrates by electrospinning and their application to solar modules. Sol Energ Mat Sol C. 2013;111:9-15.
162. Xia F, Jiang L. Bio-Inspired, Smart, Multiscale Interfacial Materials. Adv Mater. 2008 2008-08-04;20(15):2842-58.
163. Termonia Y. Molecular modeling of spider silk elasticity. Macromolecules. 1994;27(25):7378-81.
164. Nova A, Keten S, Pugno NM, Redaelli A, Buehler MJ. Molecular and nanostructural mechanisms of deformation, strength and toughness of spider silk fibrils. Nano Lett. 2010;10(7):2626-34.
165. Keten S, Buehler MJ. Nanostructure and molecular mechanics of spider dragline silk protein assemblies. Journal of the Royal Society Interface. 2010;7(53):1709-21.
166. Hayashi CY, Shipley NH, Lewis RV. Hypotheses that correlate the sequence, structure, and mechanical properties of spider silk proteins. Int J Biol Macromol. 1999;24(2):271-5.
167. Keten S, Xu Z, Ihle B, Buehler MJ. Nanoconfinement controls stiffness, strength and mechanical toughness of [beta]-sheet crystals in silk. Nature materials. 2010;9(4):359-67.
168. Gosline JM, DeMont ME, Denny MW. The structure and properties of spider silk. Endeavour. 1986;10(1):37-43.
169. Yang M, Asakura T. Design, expression and solid-state NMR characterization of silk-like materials constructed from sequences of spider silk, Samia cynthia ricini and Bombyx mori silk fibroins. J Biochem. 2005;137(6):721-9.
170. Wang M, Yu JH, Kaplan DL, Rutledge GC. Production of submicron diameter silk fibers under benign processing conditions by two-fluid electrospinning. Macromolecules. 2006;39(3):1102-7.
171. Yun Jung YANG YJY, Yoo Seong CHOI YSC, Dooyup JUNG DJ, Hyung Joon CHA HJC. Aneroin: New Sea Anemone-originated Silk Protein. The Korean Society for Biotechnology and Bioengineering. 2011:135.
172. Yang YJ, Choi YS, Jung D, et al. Production of a novel silk-like protein from sea anemone and fabrication of wet-spun and electrospun marine-derived silk fibers. NPG Asia Materials. 2013;5(6):e50.
173. Cartier O. Studien über den feineren Bau der Epidermis bei den Reptilien. II. Abt. Über die Wachsthumserscheinungen der Oberhaut von Schlangen und Eidechsen bei der Häutung, Arb. zool.-zoot. Inst. Würz. 1874;1:239-58.
174. Bhushan B. Adhesion of multi-level hierarchical attachment systems in gecko feet. J Adhes Sci Technol. 2007;21(12-13):1213-58.
175. Autumn K, Liang YA, Hsieh ST, et al. Adhesive force of a single gecko foot-hair. Nature. 2000;405(6787):681-5.
176. Prevenslik T. Electrostatic Gecko Mechanism. Tribology in Industry. 2009;31(1-2):61-6.
177. Autumn K, Sitti M, Liang YA, et al. Evidence for van der Waals adhesion in gecko setae. Proceedings of the National Academy of Sciences. 2002;99(19):12252-6.

178. Hermann Schleich H, Kastle W. Ultrastrukturen an Gecko-Zehen (Reptilia: Sauria: Gekkonidae). Amphibia-Reptilia. 1986;7(2):141-66.
179. Irschick DJ, Austin CC, Petren K, Fisher RN, Losos JB, Ellers O. A comparative analysis of clinging ability among pad-bearing lizards. Biol J Linn Soc. 1996;59(1):21-35.
180. Autumn K, Liang YA, Hsieh ST, et al. Adhesive force of a single gecko foot-hair. Nature. 2000;405(6787):681-5.
181. Parsaiyan H, Barazandeh F, Rezaei SM, Safdari M. Analytical model of adhesion for analyzing biological and synthetic nanostructured fibrillar adhesive pads. 2nd Electronics Systemintegration Technology Conference. Greenwich,UK, 2008:1153-6.
182. Chen P, McKittrick J, Meyers MAE. Biological materials: Functional adaptations and bioinspired designs. Prog Mater Sci. 2012;57(8):1492-704.
183. Bullock JM, Federle W. Division of labour and sex differences between fibrillar, tarsal adhesive pads in beetles: effective elastic modulus and attachment performance. J Exp Biol. 2009;212(12):1876-88.
184. Green DM. Adhesion and the toe-pads of treefrogs. Copeia. 1981:790-6.
185. Najem JF. Gecko-Inspired Electrospun Flexible Fiber Arrays for Adhesion: University of Akron, 2012.
186. Ballarin FM, Blackledge TA, Davis C, et al. Effect of topology on the adhesive forces between electrospun polymer fibers using a T-peel test. Polymer Engineering & Science. 2013.
187. Eadie L, Ghosh TK. Biomimicry in textiles: past, present and potential. An overview. Journal of The Royal Society Interface. 2011;8(59):761-75.
188. Weiner S, Wagner HD. The material bone: structure-mechanical function relations. Annual Review of Materials Science. 1998;28(1):271-98.
189. Li C, Jin H, Botsaris GD, Kaplan DL. Silk apatite composites from electrospun fibers. J Mater Res. 2005;20(12):3374-84.
190. Luz GM, Mano JF. Mineralized structures in nature: examples and inspirations for the design of new composite materials and biomaterials. Compos Sci Technol. 2010;70(13):1777-88.
191. Weiner S, Traub W, Wagner HD. Lamellar bone: structure--function relations. J Struct Biol. 1999;126(3):241-55.
192. Asran AS, Henning S, Michler GH. Polyvinyl alcohol--collagen--hydroxyapatite biocomposite nanofibrous scaffold: mimicking the key features of natural bone at the nanoscale level. Polymer. 2010;51(4):868-76.
193. Xie J, Li X, Lipner J, et al. "Aligned-to-random" nanofiber scaffolds for mimicking the structure of the tendon-to-bone insertion site. Nanoscale. 2010;2(6):923-6.
194. Koch K, Bhushan B, Barthlott W. Multifunctional surface structures of plants: An inspiration for biomimetics. Prog Mater Sci. 2009 2009-02-01;54(2):137-78.
195. WIGGLESWORTH VB. Transpiration through the cuticle of insects. J Exp Biol. 1945;21(3-4):97-114.
196. Liu K, Jiang L. Multifunctional Integration: From Biological to Bio-Inspired Materials. ACS Nano. 2011 2011-09-12;5(9):6786-90.